Electronic Supplementary Material (ESI) for ChemComm.

Electronic Supplementary Information

Size-matched Recognition of Large Anions by Cyanostar Macrocycles is Saved when Solvent-biased is Avoided

Bo Qiao, Joseph R. Anderson, Maren Pink, and Amar H. Flood*

Department of Chemistry, Indiana University, 800 E Kirkwood Avenue,

Bloomington, IN 40405, USA

S1. General Methods

Reagents were obtained from commercial suppliers and used as received unless otherwise noted. The two substrates of the first step, 2-(3-(hydroxymethyl)-5-iodophenyl)acetonitrile, and 1-iodo-2,6-diisopropylbenzene were prepared according to reported procedures.[1,2] Column chromatography was performed on silica gel (160–200 mesh, Sorbent Technologies, USA). Thin-layer chromatography (TLC) was performed on pre-coated silica gel plates (0.25 mm thick, #1615126, Sorbent Technologies, USA) and observed under UV light. Nuclear magnetic resonance (NMR) spectra were recorded on Varian Inova (600MHz, 500MHz, and 400 MHz) and Varian VXR (400 MHz) spectrometers at room temperature (298 K). Chemical shifts were referenced on residual solvent peaks. High-resolution electrospray ionization and electron ionization mass spectroscopy (HR-ESI-MS and HR-EI-MS) was performed on a Thermo Electron Corporation MAT 95XP-Trap mass spectrometer. Ionic impurities in target molecules were removed by extraction with deionized water. The extraction was monitored by conductivity of both the aqueous layer and the organic layer. Electrical conductivity was measured by JENCO 3010 portable conductivity meter.

S2. Computer Aided Designs of *i*PrCS

To simplify the binding stoichiometry of the cyanostar-anion complex down to 1:1, we envisioned that bulky side groups would sterically hinder the formation of the 2:1 sandwich complex. Prior to committing to synthesis, a straightforward computer-aided design approach (Figure S1) was used to evaluate how different side groups would inhibit dimer formation. Molecular mechanics (MM) became an expedient option on account of the fact that it reasonably accounts for π-π stacking, which may stem from the local view of π-π interactions promulgated by Wheeler.[3]

Molecular modeling helped identify an ideal bulky side group from among five alternatives. Our methodology (Figure S1a) employs a cyanostar derived from the original crystal structure. We fix the geometry of the core on account of the fact that molecular mechanics does not accurately reproduce the covalently bonded macrocycle's structure. However, we let the side groups relax. We then create a 2:1 sandwich around a perchlorate anion and initially position the pair of cyanostars ~3 Å from each other. Molecular mechanics was then used to optimize the entire complex resulting in increased inter-plane distances. The resulting distances between the two macrocycles were measured and compared to the distance obtained for the perchlorate crystal structure[1] of the parent cyanostar (Figure S1b). As a reference point, molecular mechanics produces an inter-plane distance of 3.8 which overestimates the 3.5 Å observed for the crystal structure. We examined benzenes with 2,6 and 3,5 substitutions either directly linked to the cyanostar core or with an acetylene linker. The inter-plane distances for these compounds suggested that an ideal bulky group is both large and close to the core of the

macrocycle. The 2,6-diisopropylphenyl substituted cyanostar (***i*PrCS**) fulfilled these criteria. With an inter-macrocycle distance of 6.0 Å, the modeling suggests that both the 2:1 sandwich complexes and self-associated species will be inhibited.

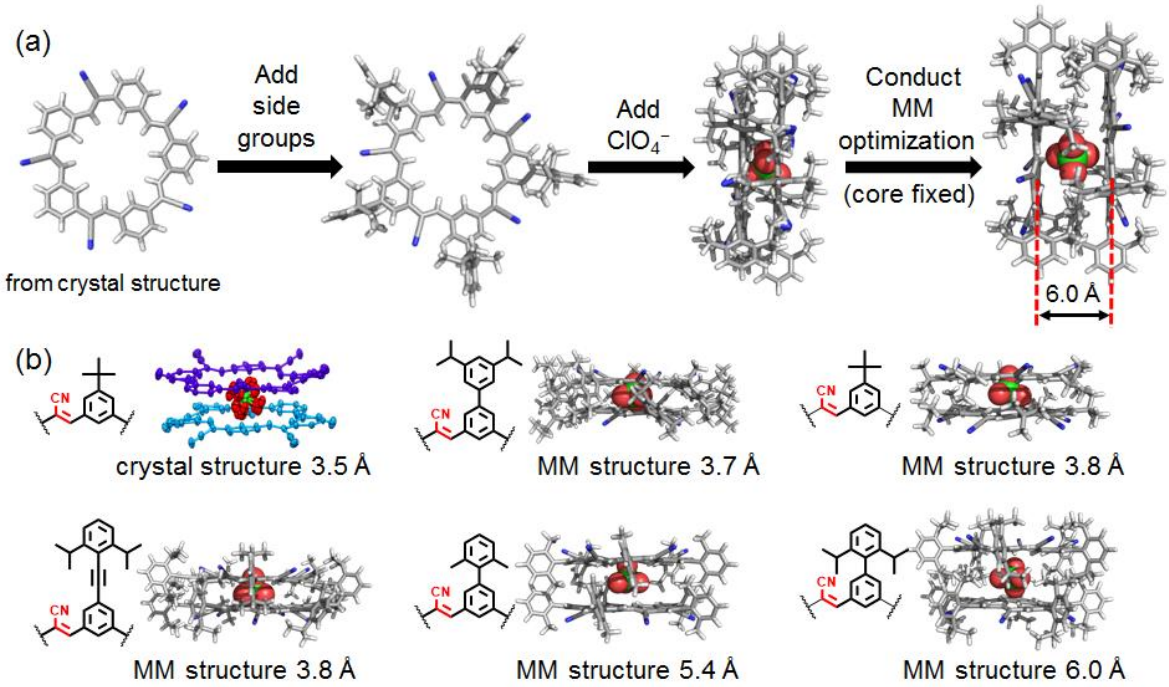

Figure S1. (a) General approach used to evaluate the impact of side groups on the distance between two macrocycles. (b) MM optimized structures and the inter plane distances for the various side groups and the perchlorate crystal structure of the parent cyanostar bearing *tert*-butyl groups.

S3. Syntheses and Compound Characterizations

List of abbreviations

$Pd(dppf)Cl_2$	[1,1′-bis(diphenylphosphino)ferrocene]dichloropalladium(II)
$Pd_2(dba)_3$	tris(dibenzylideneacetone)dipalladium(0)
SPhos	2-dicyclohexylphosphino-2′,6′-dimethoxybiphenyl
PCC	pyridinium chlorochromate
TBAI	tetrabutylammonium iodide
DMSO	dimethylsulfoxide
THF	tetrahydrofuran
EtOH	ethanol
EtOAc	ethyl acetate

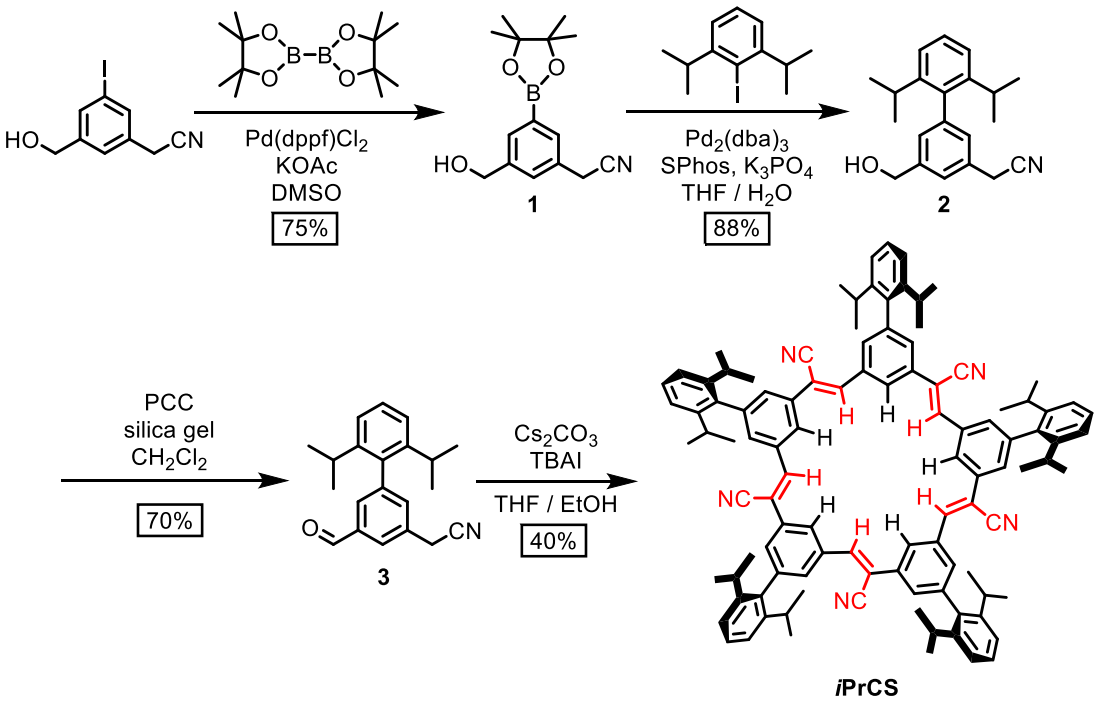

Scheme S1. Synthesis of ***i*PrCS**.

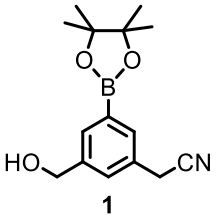

2-(3-(Hydroxymethyl)-5-(4,4,5,5-tetramethyl-1,3,2-dioxaborolan-2-yl)phenyl)acetonitrile (1): 2-(3-(Hydroxymethyl)-5-iodophenyl)acetonitrile (1.00 g, 3.66 mmol), bis(pinacolato)-diboron (1.39 g, 5.50 mmol), potassium acetate (1.08 g, 11.0 mmol), and Pd(dppf)Cl_2 (80 mg, 0.10 mmol) were placed in a round bottom flask. The flask was degassed with argon. DMSO (40 mL) was added to the flask via syringe. The solution was stirred at 70 °C for 12 h. The reaction was quenched by brine and washed with EtOAC (50 mL × 3). The organic phase was combined and dried over Na_2SO_4 and concentrated in vacuo. Column chromatography over silica gel (hexane:EtOAc = 2:1) yielded boronic ester **1** (750 mg, 2.74 mmol, 75%) as a colorless oil. ^{1}H NMR ($CDCl_3$, 500 MHz), δ = 7.75 (s, 1H), 7.67 (s, 1H), 7.48 (s, 1H), 4.72 (d, J = 4.5 Hz, 2H), 3.75 (s, 2H), 1.74 (t, J = 4.5 Hz, 1H), 1.35 (s, 12H). ^{13}C NMR (CDCl3, 100 MHz), δ = 141.3, 133.4, 132.8, 129.6, 129.2, 117.8, 84.1, 64.7, 24.8, 23.4. HR-EI-MS: $C_{15}H_{20}O_3NB$ M^+, Calculated: 273.1531, Found: 273.1525.

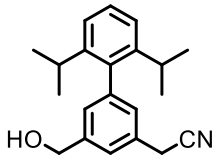

2

2-(5-(Hydroxymethyl)-2',6'-diisopropyl-[1,1'-biphenyl]-3-yl)acetonitrile (2): Boronic ester **1** (453 mg, 1.66 mmol), 1-iodo-2,6-diisopropylbenzene (573 mg, 1.99 mmol), potassium phosphate (tribasic, 1.06 g, 5 mmol), $Pd_2(dba)_3$ (75 mg, 0.082 mmol), and SPhos (68 mg, 0.16 mmol) were placed in a round bottom flask. The flask was degassed with argon. THF (10 mL) and water (10 mL) were added into the flask via syringe. The reaction mixture was allowed to stir at 60 °C for 12 h and then extracted with EtOAc (30 mL × 3). The organic phase was dried over Na_2SO_4 and concentrated in vacuo. Column chromatography over silica gel (hexane:EtOAc = 8:1) yielded benzyl alcohol **2** (450 mg, 1.46 mmol, 88%) as a white solid. ^{1}H NMR ($CDCl_3$, 400 MHz), δ = 7.37 (s, 1H), 7.35 (t, *J* = 7.8 Hz, 1H), 7.21 (*d*, J = 7.7 Hz, 2H), 7.13 (s, 1H), 7.07 (s, 1H), 4.77 (d, *J* = 5.6 Hz, 2H), 3.81 (s, 2H), 2.52 (septet, *J* = 6.9 Hz, 2H), 1.76 (t, *J* = 5.7 Hz, 1H), 1.08 (d, *J* = 6.8 Hz, 12H). ^{13}C NMR ($CDCl_3$, 100 MHz) δ = 146.6, 142.1, 141.8, 138.3, 130.0, 128.2, 127.6, 124.6, 122.6, 117.8, 75.0, 64.8, 30.3, 24.2, 23.7. HR-EI-MS: $C_{21}H_{25}ON$ M^+, Calculated: 307.1931, Found: 307.1923.

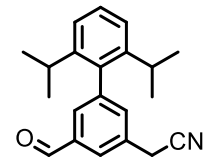

3

2-(5-Formyl-2',6'-diisopropyl-[1,1'-biphenyl]-3-yl)acetonitrile (3): PCC (460 mg, 2.18 mmol) and silica gel (2.0 g) were mixed using a mortar and pestle and suspended in CH_2Cl_2 (20 mL). A solution of benzyl alcohol **2** (418 mg, 1.36 mmol) in CH_2Cl_2 (10 mL) was dropwise added into the PCC suspension while stirring. The reaction mixture was stirred for 12 h at room temperature and filtered through a short silica gel column (hexane:EtOAC = 8:1) to yield benzaldehyde **3** as a white solid (288 mg, 0.94 mmol, 70%). ^{1}H NMR ($CDCl_3$, 400 MHz), δ = 10.07 (s, 1H), 7.87 (s, 1H), 7.68 (s, 1H), 7.45 (s, 1H), 7.39 (t, *J* = 7.6 Hz, 1H), 7.23 (d, *J* = 7.7 Hz, 2H), 3.90 (s, 2H), 2.45 (septet, *J* = 6.9 Hz, 2H), 1.09 (d, *J* = 6.8 Hz, 6H), 1.08 (d, *J* = 6.8 Hz, 6H). ^{13}C NMR ($CDCl_3$, 100 MHz), δ = 191.4, 146.5, 143.1, 137.0, 136.9, 134.7, 131.1, 130.8, 128.7, 127.0, 122.8, 117.0, 30.4, 24.1, 23.6. HR-EI-MS: $C_{21}H_{23}ON$ M^+, Calculated: 305.1774, Found: 305.1768

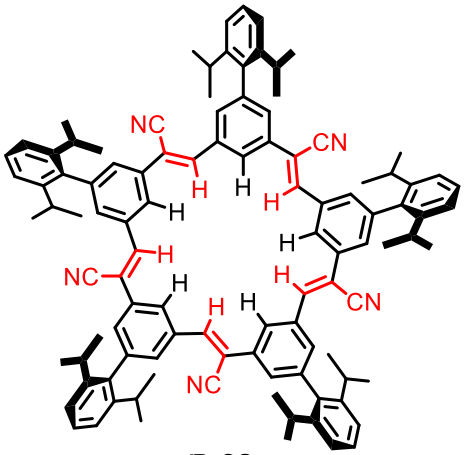

***i*PrCS**

Penta(2,6-diisopropylphenyl)-cyanostar (*i*PrCS): A suspension of cesium carbonate (310 mg, 0.95 mmol) in EtOH (120 mL) was stirred at 50 °C until the salt was fully dissolved and then added THF (100 mL). The mixture was cooled to room temperature, charged with TBAI (180 mg, 0.49 mmol), and degassed with argon for 10 min. A solution of benzaldehyde **3** (291 mg, 0.95 mmol) in THF (20 mL) was added into the degassed solution via syringe. The reaction mixture was stirred at room temperature under dark for 12 h, concentrated in vacuo, re-suspended in CH_2Cl_2, and filtered to remove excess of Cs_2CO_3. The resulting CH_2Cl_2 solution was washed with deionized water (10 mL × 2), dried over Na_2SO_4, and concentrated in vacuo. Column chromatography over silica gel (hexane:$CHCl_3$ = 2:1) yielded the cyanostar ***i*PrCS** (110 mg, 0.076 mmol, 40%) as a white solid. ^{1}H NMR (CD_2Cl_2, 600 MHz), δ = 8.37 (s, 5H), 7.99 (s, 5H), 7.97 (s, 5H), 7.68 (s, 5H), 7.39 (t, J = 7.8 Hz, 5H), 7.25 (d, J = 7.8 Hz, 10H), 2.63 (septet, J = 6.8, 10H), 1.14 (d, J = 6.8, 30H), 1.12 (d, J = 6.8, 30H). ^{13}C NMR (CD_2Cl_2, 125 MHz) δ = 146.6, 143.4, 141.4, 137.5, 134.8, 134.0, 130.9, 128.6, 128.1, 127.0, 122.8, 116.8, 111.6, 30.6, 24.0, 23.9. HR-ESI-MS: $C_{105}H_{105}N_5I$ $[M + I]^-$, Calculated: 1562.7415, Found: 1562.7454.

S4. X-Ray Diffraction Data Analysis of *i*PrCS

Data Collection

The data collection was carried out using synchrotron radiation (λ = 0.41328 Å, E = 30 keV, silicon 111 and 113 monochromators, two mirrors to exclude higher harmonics, slit size 100 × 100 μm) with a frame time of 1 second and a detector distance of 80 mm. A randomly oriented region of reciprocal space was surveyed to the extent of a hemisphere; details are below.

Axis	2θ/°	ω/°	φ/°	χ/°	Frames
Phi	-8.00	180.00	0.00	54.74	540
Phi	-8.00	220.00	0.00	54.74	237

The total exposure time was 0.22 hours. The frames were integrated with the Bruker SAINT software package[4] using a narrow-frame algorithm. The integration of the data using an orthorhombic unit cell yielded a total of 138045 reflections to a maximum θ angle of 14.42° (0.83 Å resolution), of which 18280 were independent (average redundancy 7.552, completeness = 96.3%, Rint = 8.23%, Rsig = 6.52%) and 9871 (54.00%) were greater than 2σ(F2). The final cell constants of a = 32.7197(18) Å, b = 16.1960(8) Å, c = 39.107(2) Å, volume = 20723.9(19) Å^3, are based upon the refinement of the XYZ-centroids of 9944 reflections above 20 σ(I) with 4.583° < 2θ < 26.31°. Data were corrected for absorption effects using the multi-scan method (SADABS).[5] The ratio of minimum to maximum apparent transmission was 0.841. The calculated minimum and maximum transmission coefficients (based on crystal size) are 0.6254 and 0.7438. Diffraction intensity strongly falls off at a resolution beyond 1 Å, which is consistent with effects of whole molecule disorder and solvent loss. Thus, data are incomplete at high resolution.

Structure Solution and Refinement

The space group Pbca was determined based on intensity statistics and systematic absences. The structure was solved using and refined using the Shelx suite of programs.[6] An intrinsic methods solution was calculated, which provided most non-hydrogen atoms from the E-map. Full-matrix least squares / difference Fourier cycles were performed, which located the remaining non-hydrogen atoms. All non-hydrogen atoms were refined with anisotropic displacement parameters, with the exception of those belonging to methanol solvent. The hydrogen atoms were placed in ideal positions and refined as riding atoms with relative isotropic displacement parameters. Shelx/SWAT was used to model diffuse solvent using Babinet's principle.[7] The final anisotropic full-matrix least-squares refinement on F2 with 1354 variables converged at R1 = 14.24%, for the observed data and wR2 = 45.60% for all data. The goodness-of-fit was 1.636. The largest peak in the final difference electron density synthesis was 1.057 e$^-$

$Å^{-3}$ and the largest hole was -0.646 e^{-} $Å^{-3}$ with an RMS deviation of 0.105 e^{-} $Å^{-3}$. On the basis of the final model, the calculated density was 0.942 g cm^{-3} and F(000), 6304 e^{-}. The structure has solvent accessible voids totaling to 4078.3 $Å^3$, which is ca. 20% of the unit cell.[8] Methanol was refined with partial sites to model the most pronounced (albeit weak) electron density in the voids. Yet likely, more solvent is present.

Acknowledgements for the Crystallography Data

ChemMatCARS Sector 15 is principally supported by the Divisions of Chemistry (CHE) and Materials Research (DMR), National Science Foundation, under grant number NSF/CHE-1346572. Use of the Advanced Photon Source, an Office of Science User Facility operated for the U.S. Department of Energy (DOE) Office of Science by Argonne National Laboratory, was supported by the U.S. DOE under Contract No. DE-AC02-06CH11357.

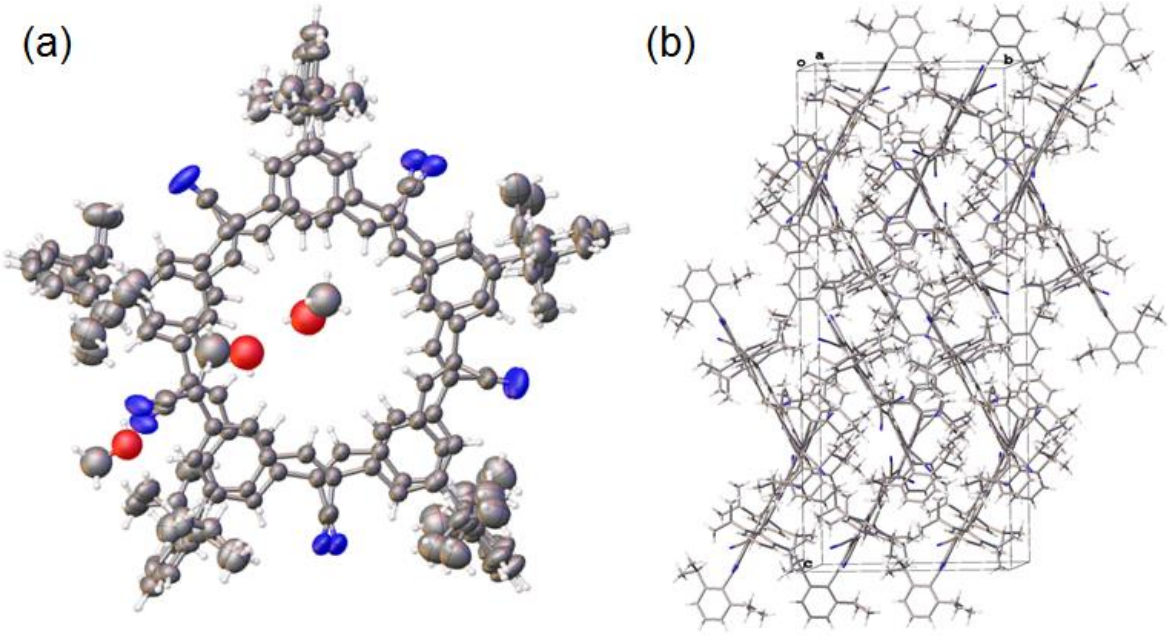

Figure S2. (a) Formula unit of the ***i*PrCS** crystal, highlighting whole molecular disorder. (b) Cell plot viewed along *a* axis. Disorder and solvent are omitted.

Table S1. Crystal data and structure refinement.

Empirical formula	$C_{106}\ H_{109}\ N_5\ O$	
Formula weight	1468.98	
Crystal color, shape, size	colorless block, 0.021 × 0.017 × 0.013 mm^3	
Temperature	230(2) K	
Wavelength	0.41328 Å	
Crystal system, space group	Orthorhombic, Pbca	
Unit cell dimensions	a = 32.7197(18) Å	α = 90°.
	b = 16.1960(8) Å	β = 90°.
	c = 39.107(2) Å	γ = 90°.
Volume	20723.7(19) $Å^3$	
Z	8	
Density (calculated)	0.942 mg/m^3	
Absorption coefficient	0.026 mm^{-1}	
F(000)	6304	

Data collection

Diffractometer	D8 Platform, ChemMatCARS, APS 15-ID-B
Theta range for data collection	0.705 to 14.417°.
Index ranges	$-38 \le h \le 39$, $-14 \le k \le 18$, $-47 \le l \le 46$
Reflections collected	138045
Independent reflections	18280 [R(int) = 0.0823]
Observed Reflections	9871
Completeness to theta = 14.357°	96.5 %

Solution and Refinement

Absorption correction	Semi-empirical from equivalents
Max. and min. transmission	0.7438 and 0.6254
Solution	Intrinsic methods
Refinement method	Full-matrix least-squares on F^2
Weighting scheme	$w = [\sigma^2 F_o^2 + AP^2]^{-1}$, with
	$P = (F_o^2 + 2\ F_c^2)/3$, A = 0.2000
Data / restraints / parameters	18280 / 4499 / 1354
Goodness-of-fit on F^2	1.636
Final R indices [I > 2sigma(I)]	$R1$ = 0.1424, $wR2$ = 0.4141
R indices (all data)	$R1$ = 0.2147, $wR2$ = 0.4560
Largest diff. peak and hole	1.057 and −0.646 $eÅ^{-3}$

Goodness-of-fit = $[\Sigma w(F_o^2 - F_c^2)^2 / (N_{observns} - N_{params})]^{1/2}$, all data.

$R1 = \Sigma(|F_o| - |F_c|) / \Sigma |F_o|$. $wR2 = [\Sigma w(F_o^2 - F_c^2)^2 / \Sigma w(F_o^2)^2]^{1/2}$.

S5. Variable Concentration Spectra of *i*PrCS

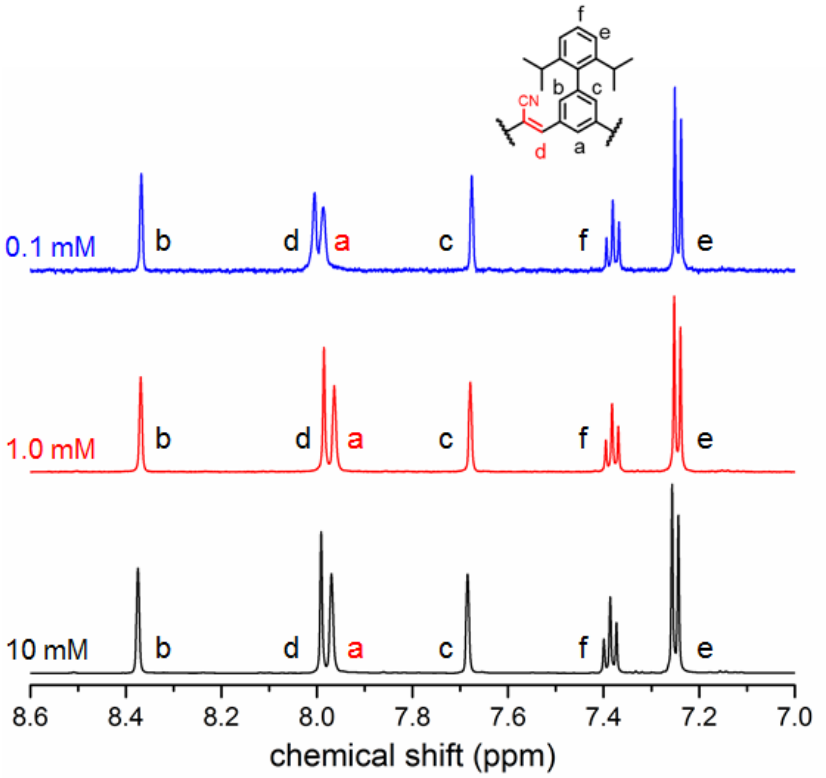

Figure S3. ^{1}H NMR spectra of ***i*PrCS** at various concentrations (CD_2Cl_2, 298 K, 600 MHz).

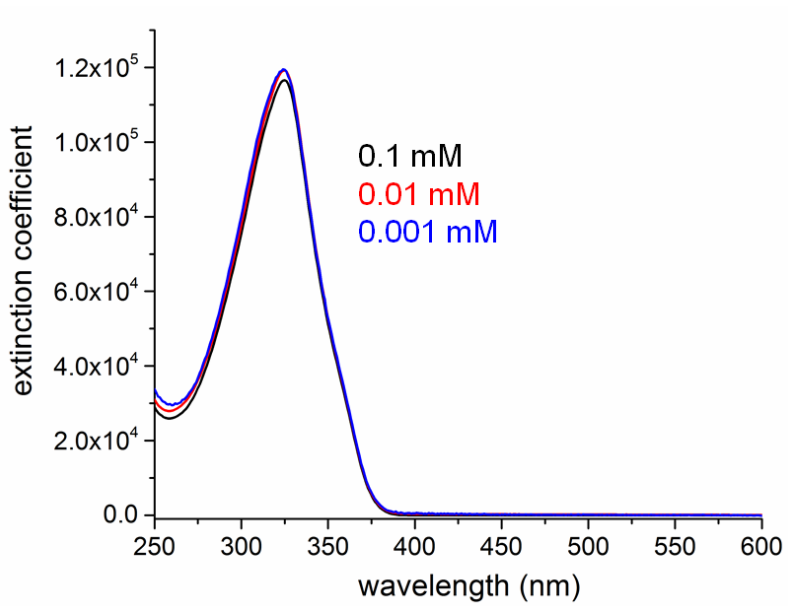

Figure S4. UV-Vis absorption spectra of ***i*PrCS** at 0.1, 0.01, and 0.001 mM in CH_2Cl_2 (absorbance was divided by concentration and path length to give extinction coefficient).

S6. Diffusion NMR Study of *i*PrCS

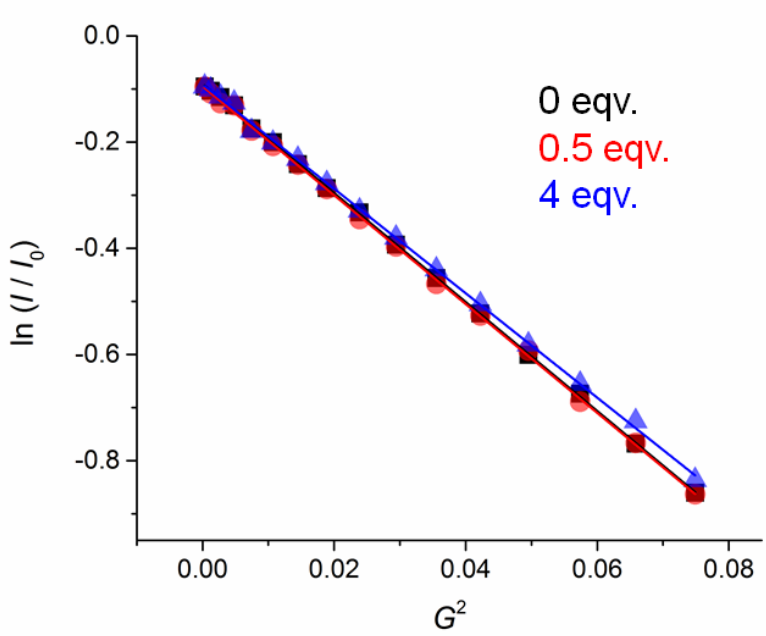

Figure S5. The ^{1}H NMR peak integration (ln [I / I_0]) of isopropyl protons (60H) on ***i*PrCS** as a function of gradient field strength (G^2) with increasing equivalents (0, 0.5, and 4) of $TBAClO_4$ (1 mM, 40:60 CD_3OD:CD_2Cl_2, 298 K, 600 MHz).

Diffusion coefficients (D) of ***i*PrCS** with various equivalents (0, 0.5, and 4) of tetrabutylammonium perchlorate, $TBAClO_4$ were obtained by fitting the ^{1}H NMR peak intensity of the strong isopropyl signal as a function of gradient field strength (Figure S5). The almost constant diffusion coefficient (Table S2) is consistent with the formation of 1:1 species and the absence of 2:1 and other higher order species. The slightly slower diffusion at 4 equivalents is presumably due to the change in viscosity with the addition of $TBAClO_4$ salt.

Table S2. The diffusion coefficients (D) of ***i*PrCS** with various equivalents of $TBAClO_4$ (1 mM, 40:60 *v*/*v* CD_3OD:CD_2Cl_2, 298 K)

$TBAClO_4$ equivalents	D ($\times 10^{-10}$ m^2 s^{-1})
0	4.99 ±0.03
0.5	4.98 ±0.03
4	4.78 ±0.06

S7. Estimation of the Cavity Size of Cyanostar

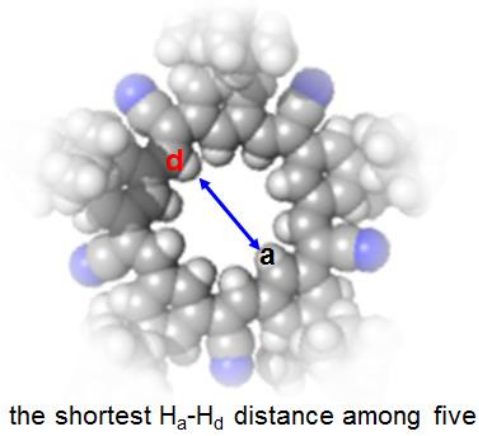

Figure S6. Cross-cavity distance of cyanostar to be used in estimating the cavity size.

The cavity size of cyanostar is estimated (Figure S6) based on the shortest cross-cavity Ha-H_d distance (6.7 Å, obtained from crystal structure) minus two van der Waals radii of hydrogen atom (1.1 Å). The result is 4.5 Å.[9]

S8. NMR Titrations and Anion Binding Analysis of *i*PrCS

Methods

A typical anion titration (for example, tetrabutylammonium chloride, TBACl) with the macrocycle is as follows: A solution of the receptor ***i*PrCS** (500 μL, 1 mM, 40:60 CD_3OD:CD_2Cl_2) was placed in an NMR tube sealed with a rubber septum. An initial ^{1}H NMR spectrum was recorded and additional spectra were obtained after aliquots of a TBACl solution (25 mM, 40:60 CD_3OD:CD_2Cl_2) was injected sequentially using a microsyringe.

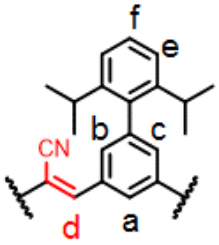

Figure S7. Chemical structure of ***i*PrCS** with protons labeled

The concentrations of ***i*PrCS** and TBACl at each point during the titration were then calculated based on the initial concentrations and the volume of TBACl solution added. The concentration data along with the ^{1}H NMR chemical shift positions of the two protons inside the macrocycle's binding cavity (Figure S7, H_a and H_d) were then fitted according to the proposed 1:1 binding model (Equation 1) using HypNMR 2008.[10] Other protons were not included in the fitting because the changes in their chemical shift positions are much smaller compared to H_a and H_d.

$$\textbf{\textit{i}PrCS} + X^- \rightleftharpoons \textbf{\textit{i}PrCS}\bullet X^- \qquad (1)$$

The ion pairing between the counter cation tetrabutylammonium (TBA^+) with anionic species (X^- and/or ***i*PrCS**•X^-) was not included on account of the negligible chemical shift change of the TBA^+ protons during all titrations (See figures below for peak positions of TBA^+ α-proton).

Goodness of fit was established from the fitting residuals and the sigma values. A good fitting typically has residual less than 0.02 ppm for all data points and sigma less than 10. Errors were estimated by the fitting tool based on fitting residuals. For good fittings with less than 0.02 ppm residuals for all data points, the errors on log *K* values are usually less than 1%. For some anions (*i.e.*, Br^-, BF_4^-, NO_3^-, ClO_4^-, and I^- in CD_3CN:CD_2Cl_2; as well as I^- and ClO_4^- in CD_3OD:CD_2Cl_2), the fittings are too poor at 1 mM on account of their strong affinity. This assessment is based on the fact that fitted chemical shifts have significant residuals compared to experimental data and sigma values are greater than 15. These titrations were repeated at a lower 0.1 mM concentration and the goodness of fit was seen to improve. For example, iodide at 1 and 0.1 mM, the sigma values and estimated errors changes from 15 and 3% to 6.3 and 0.2%. Data fitting was independently corroborated using an online fitting tool Bindfit.[11,12] The data sets and fitting results are available online – see the list of URLs following:

Bindfit URL List of Titrations in 40:60 CD_3OD:CD_2Cl_2

TBACl
http://app.supramolecular.org/bindfit/view/eca885ac-ffb9-41a1-b453-39ee1afc211e
TBABr
http://app.supramolecular.org/bindfit/view/7cfc7816-ed79-4791-b428-976b9017bf03
$TBANO_3$
http://app.supramolecular.org/bindfit/view/ebe26b20-4b79-4c87-b783-25d631e8299c
$TBABF_4$
http://app.supramolecular.org/bindfit/view/9f2240bd-85dd-4779-b6de-674b7411748e
TBAI
http://app.supramolecular.org/bindfit/view/fc41ddb3-ba7c-461b-afc7-d8dcdd27d724
$TBAClO_4$
http://app.supramolecular.org/bindfit/view/73837036-61d0-4be9-95ff-714ae86790e0

$TBAReO_4$
http://app.supramolecular.org/bindfit/view/67502878-5194-45b0-acf1-239f7ab295ab
$TBAIO_4$
http://app.supramolecular.org/bindfit/view/8963acb0-ae72-403a-afb1-a75e73269760
$TBAPF_6$
http://app.supramolecular.org/bindfit/view/8c412695-f8f1-42d4-b6c8-ecde0a395aa6
$TBASbF_6$
http://app.supramolecular.org/bindfit/view/c8196a1c-b79c-4b47-b6a2-234baa69db13

Bindfit URL List Titrations in 50:50 CD_3CN:CD_2Cl_2
TBACl
http://app.supramolecular.org/bindfit/view/53758528-f03e-4ecb-b389-0b8302279438
TBABr
http://app.supramolecular.org/bindfit/view/ca6cedcc-cc49-4e2a-a029-0005fe5b6c70
$TBANO_3$
http://app.supramolecular.org/bindfit/view/f69ec38b-0b86-4cda-9b16-a13b61a9f846
$TBABF_4$
http://app.supramolecular.org/bindfit/view/2dd35183-9200-4472-ba7f-8330f3a27d96
TBAI
http://app.supramolecular.org/bindfit/view/47558fd9-5527-4256-b0d5-751a512b5765
$TBAClO_4$
http://app.supramolecular.org/bindfit/view/b690f5e0-81b1-4aa1-8bf7-f839d9a7df5c
$TBAReO_4$
http://app.supramolecular.org/bindfit/view/b985e0a5-ef8b-4655-8b33-f43ac82f6e72
$TBAIO_4$
http://app.supramolecular.org/bindfit/view/f3d82211-5f0c-4120-9b60-ae028071c7b3
$TBAPF_6$
http://app.supramolecular.org/bindfit/view/863c9831-47e2-4067-84b2-2f24fefda64c
$TBASbF_6$
http://app.supramolecular.org/bindfit/view/98aaf0fa-72c1-4856-a790-e8b9340c80aa

Binding Data and Fitting Results in the 40:60 *v/v* Methanol:Dichloromethane Mixture

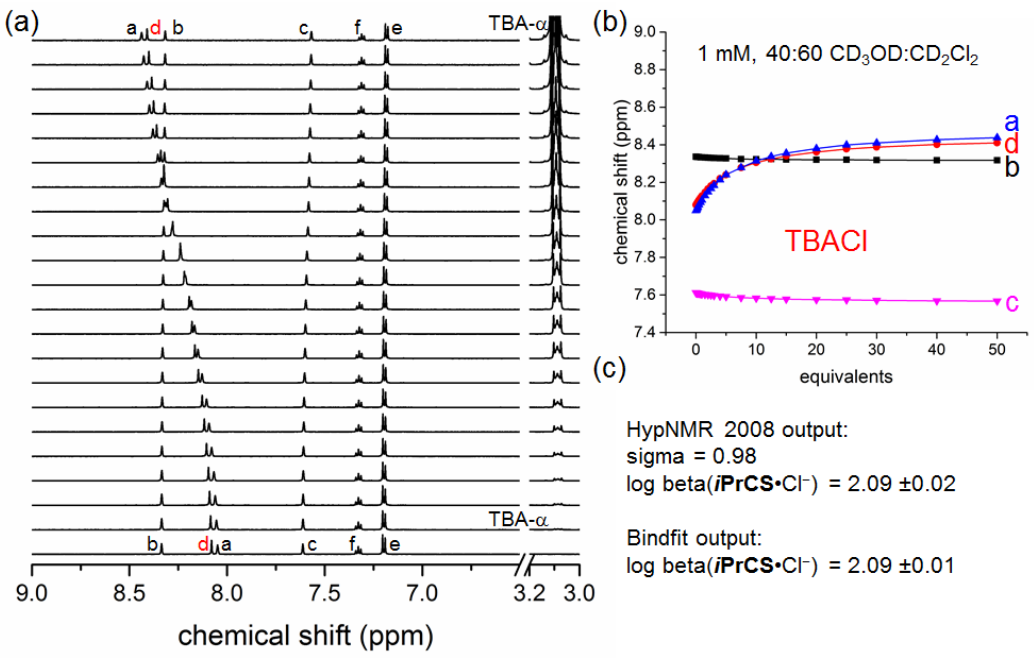

Figure S8. (a) Stacked ^{1}H NMR spectra and (b) cyanostar core protons' chemical shift positions connected by trend lines with increasing amount of TBACl (1 mM ***i*PrCS**, 40:60 CD_3OD:CD_2Cl_2, 298 K, 600 MHz). (c) Fitting output from HypNMR 2008 and Bindfit.

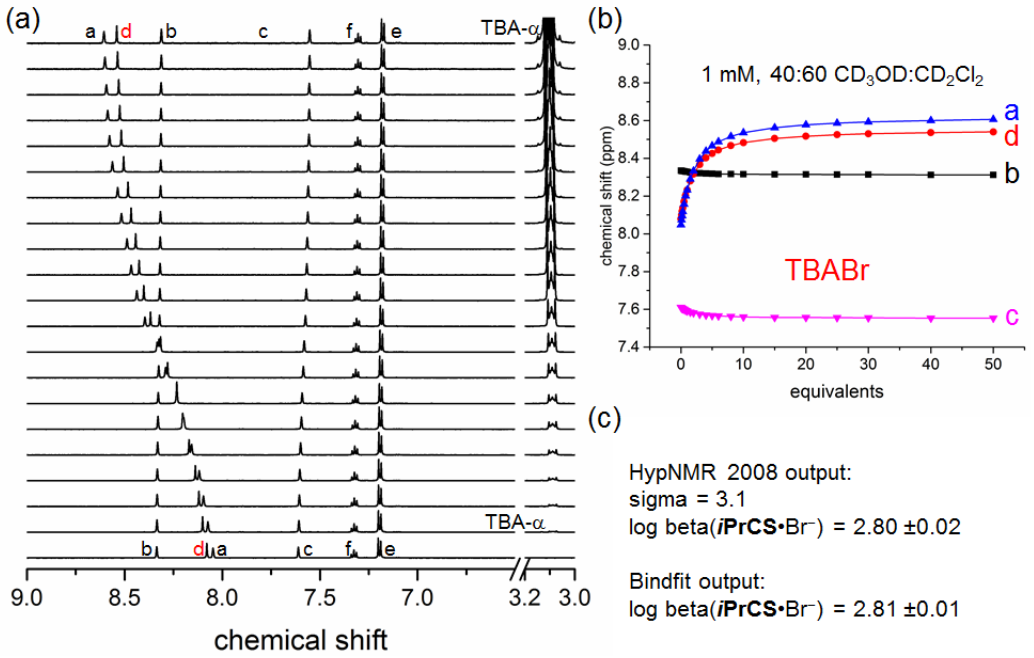

Figure S9. (a) Stacked ^{1}H NMR spectra and (b) cyanostar core protons' chemical shift positions connected by trend lines with increasing amount of TBABr (1 mM ***i*PrCS**, 40:60 CD_3OD:CD_2Cl_2, 298 K, 600 MHz). (c) Fitting output from HypNMR 2008 and Bindfit.

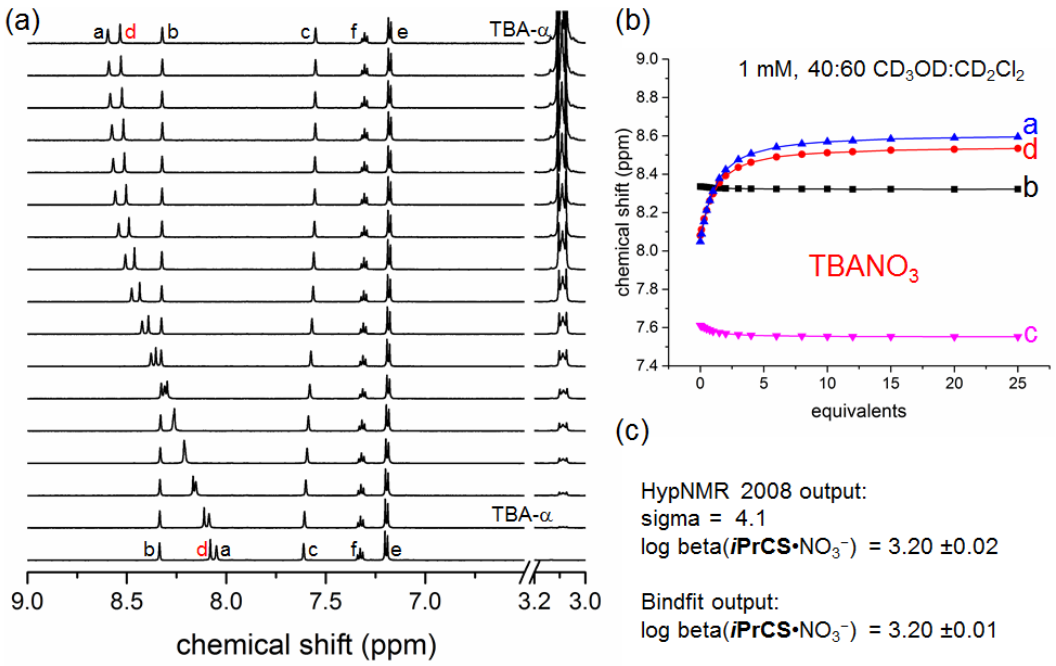

Figure S10. (a) Stacked ^{1}H NMR spectra and (b) cyanostar core protons' chemical shift positions connected by trend lines with increasing amount of $TBANO_3$ (1 mM ***i*PrCS**, 40:60 CD_3OD:CD_2Cl_2, 298 K, 600 MHz). (c) Fitting output from HypNMR 2008 and Bindfit.

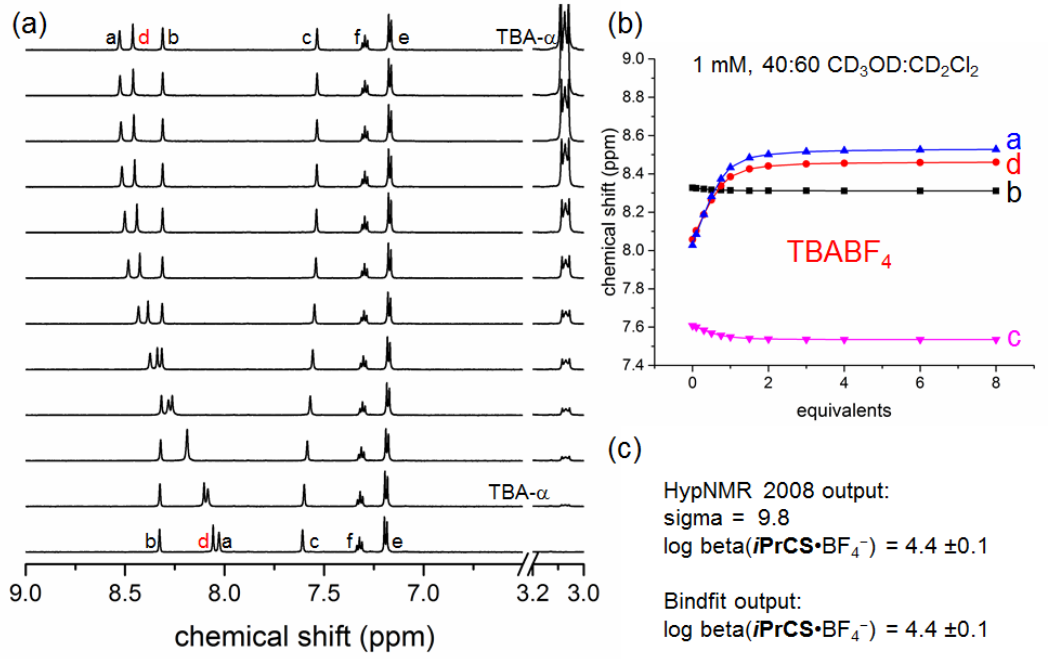

Figure S11. (a) Stacked ^{1}H NMR spectra and (b) cyanostar core protons' chemical shift positions connected by trend lines with increasing amount of $TBABF_4$ (1 mM ***i*PrCS**, 40:60 CD_3OD:CD_2Cl_2, 298 K, 600 MHz). (c) Fitting output from HypNMR 2008 and Bindfit.

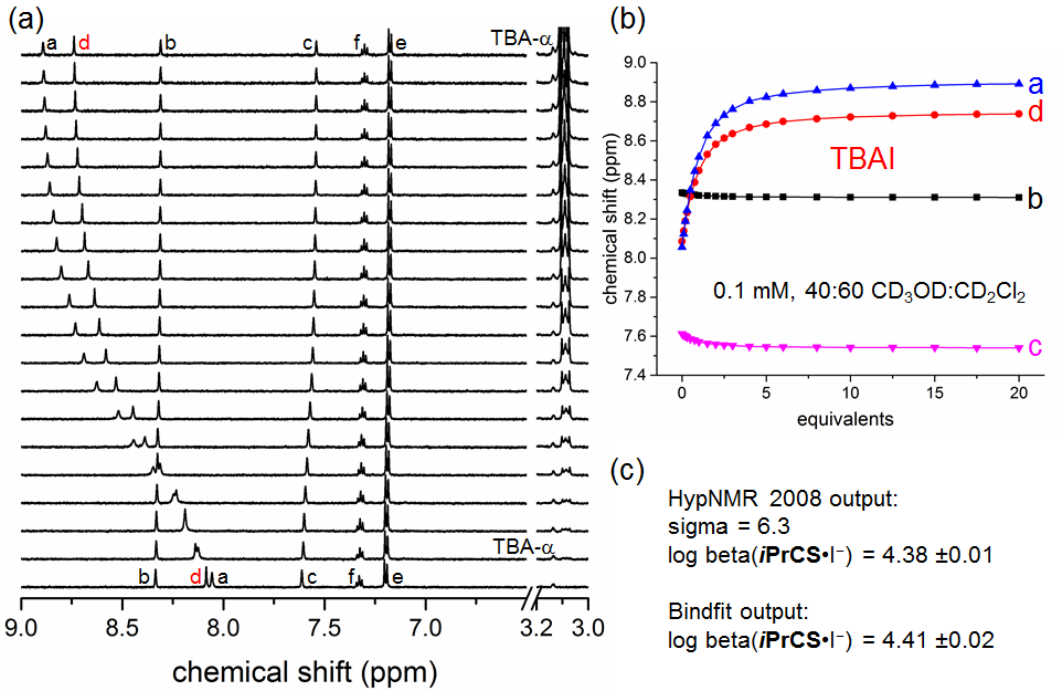

Figure S12. (a) Stacked ^{1}H NMR spectra and (b) cyanostar core protons' chemical shift positions connected by trend lines with increasing amount of TBAI (0.1 mM ***i*PrCS**, 40:60 CD_3OD:CD_2Cl_2, 298 K, 600 MHz) (c) HypNMR 2008 output for fitting the titration.

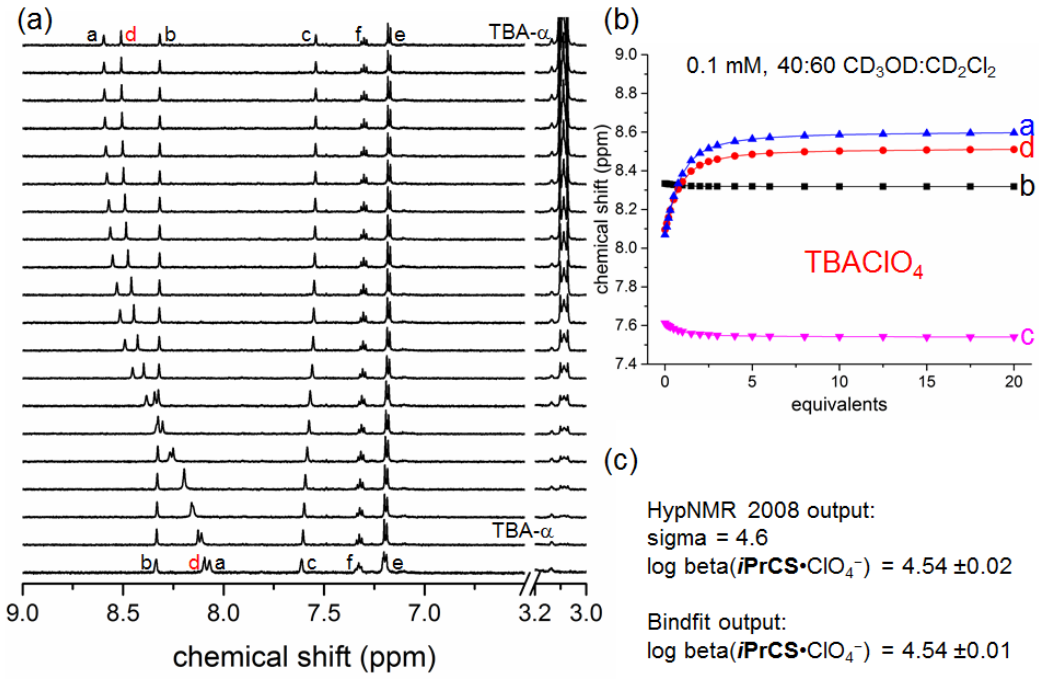

Figure S13. (a) Stacked ^{1}H NMR spectra and (b) cyanostar core protons' chemical shift positions connected by trend lines with increasing amount of $TBAClO_4$ (0.1 mM ***i*PrCS**, 40:60 CD_3OD:CD_2Cl_2, 298 K, 600 MHz). (c) Fitting output from HypNMR 2008 and Bindfit.

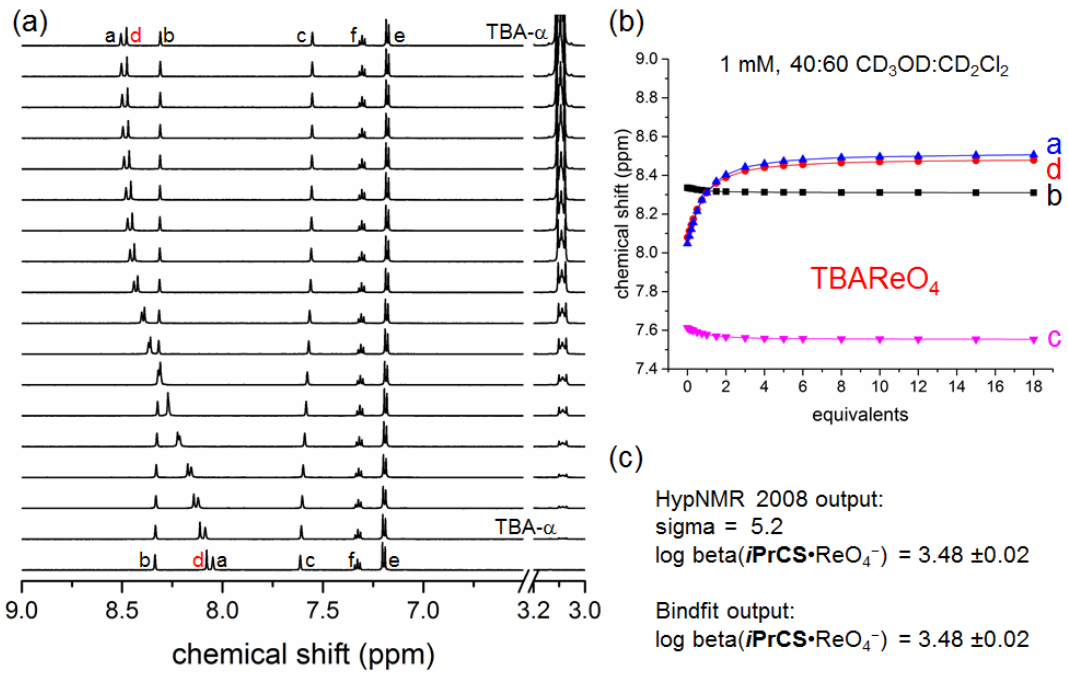

Figure S14. (a) Stacked ^{1}H NMR spectra and (b) cyanostar core protons' chemical shift positions connected by trend lines with increasing amount of $TBAReO_4$ (1 mM ***i*PrCS**, 40:60 $CD_3OD:CD_2Cl_2$, 298 K, 600 MHz). (c) Fitting output from HypNMR 2008 and Bindfit.

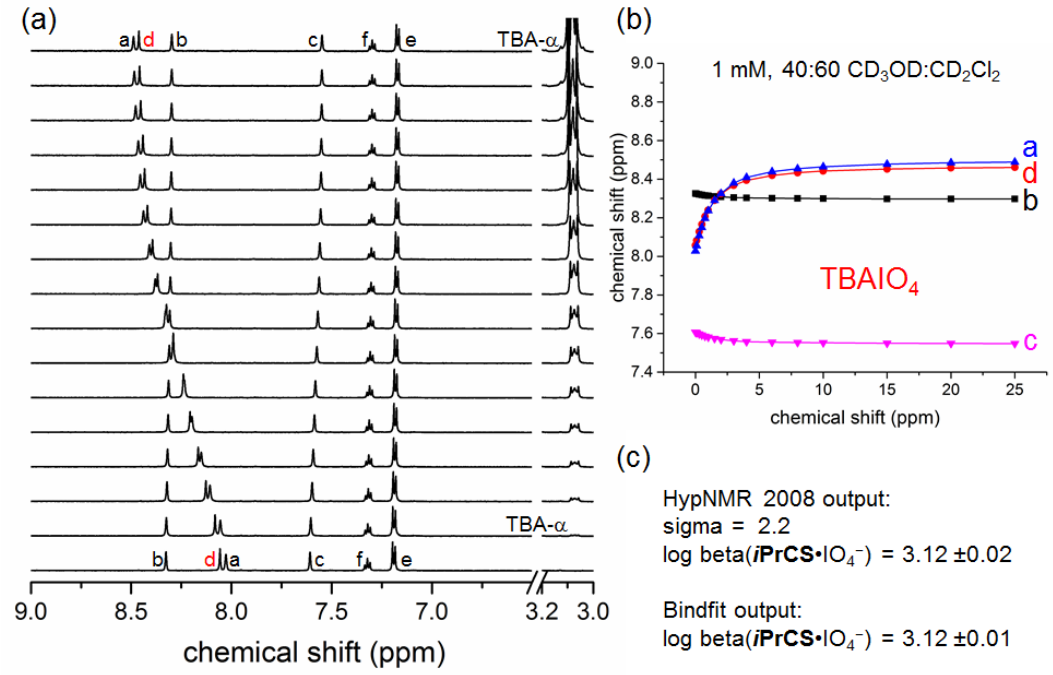

Figure S15. (a) Stacked ^{1}H NMR spectra and (b) cyanostar core protons' chemical shift positions connected by trend lines with increasing amount of $TBAIO_4$ (1 mM ***i*PrCS**, 40:60 $CD_3OD:CD_2Cl_2$, 298 K, 600 MHz). (c) Fitting output from HypNMR 2008 and Bindfit.

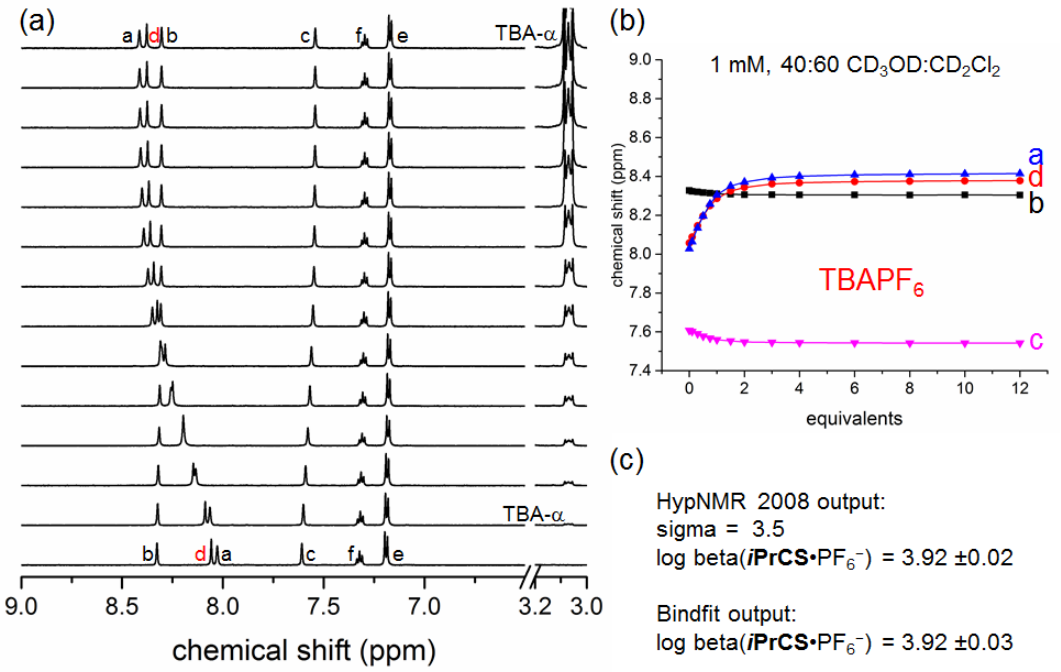

Figure S16. (a) Stacked ^{1}H NMR spectra and (b) cyanostar core protons' chemical shift positions connected by trend lines with increasing amount of $TBAPF_6$ (1 mM ***i*PrCS**, 40:60 CD_3OD:CD_2Cl_2, 298 K, 600 MHz). (c) Fitting output from HypNMR 2008 and Bindfit.

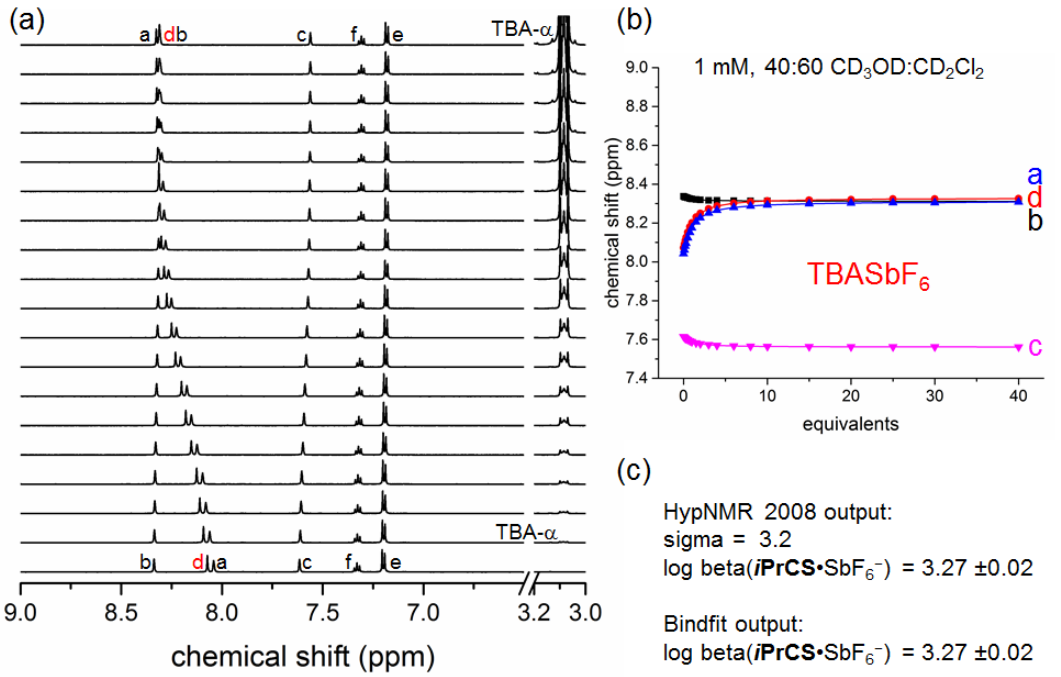

Figure S17. (a) Stacked ^{1}H NMR spectra and (b) cyanostar core protons' chemical shift positions connected by trend lines with increasing amount of $TBASbF_6$ (1 mM ***i*PrCS**, 40:60 CD_3OD:CD_2Cl_2, 298 K, 600 MHz). (c) Fitting output from HypNMR 2008 and Bindfit.

Binding Data and Fitting Results in the 50:50 *v/v* Acetonitrile:Dichloromethane Mixture

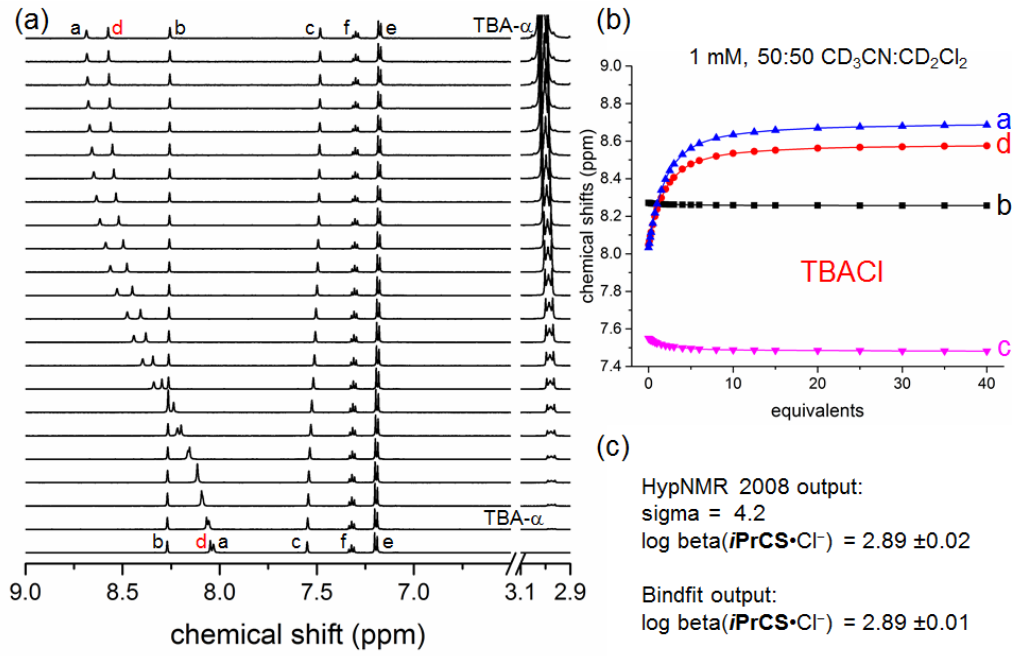

Figure S18. (a) Stacked ^{1}H NMR spectra and (b) cyanostar core protons' chemical shift positions connected by trend lines with increasing amount of TBACl (1 mM ***i*PrCS**, 50:50 CD_3CN:CD_2Cl_2, 298 K, 600 MHz). (c) Fitting output from HypNMR 2008 and Bindfit.

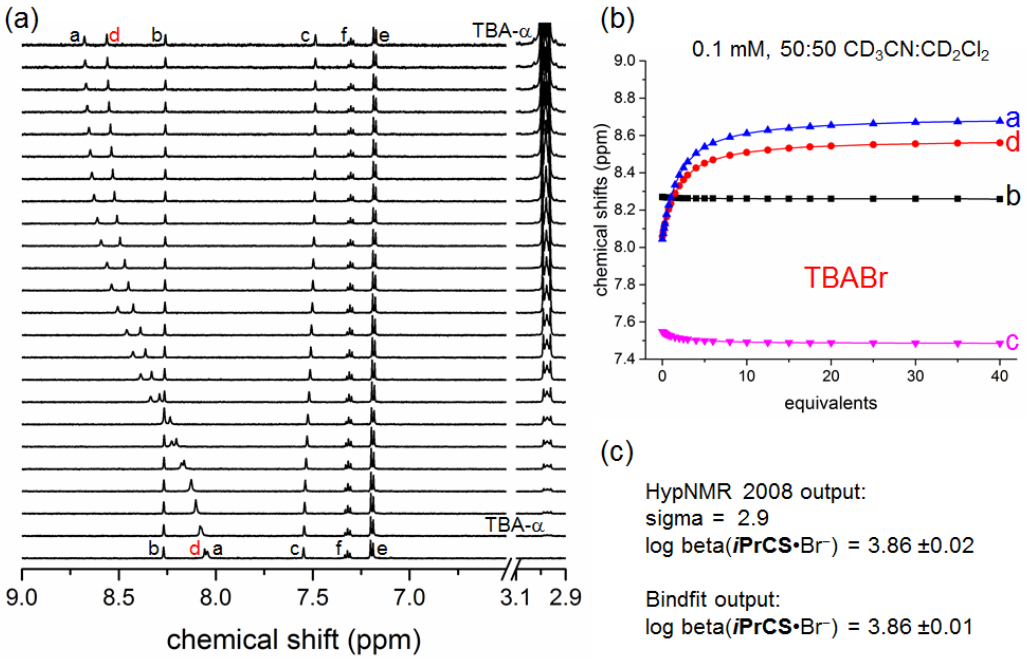

Figure S19. (a) Stacked ^{1}H NMR spectra and (b) cyanostar core protons' chemical shift positions connected by trend lines with increasing amount of TBABr (1 mM ***i*PrCS**, 50:50 CD_3CN:CD_2Cl_2, 298 K, 600 MHz). (c) Fitting output from HypNMR 2008 and Bindfit.

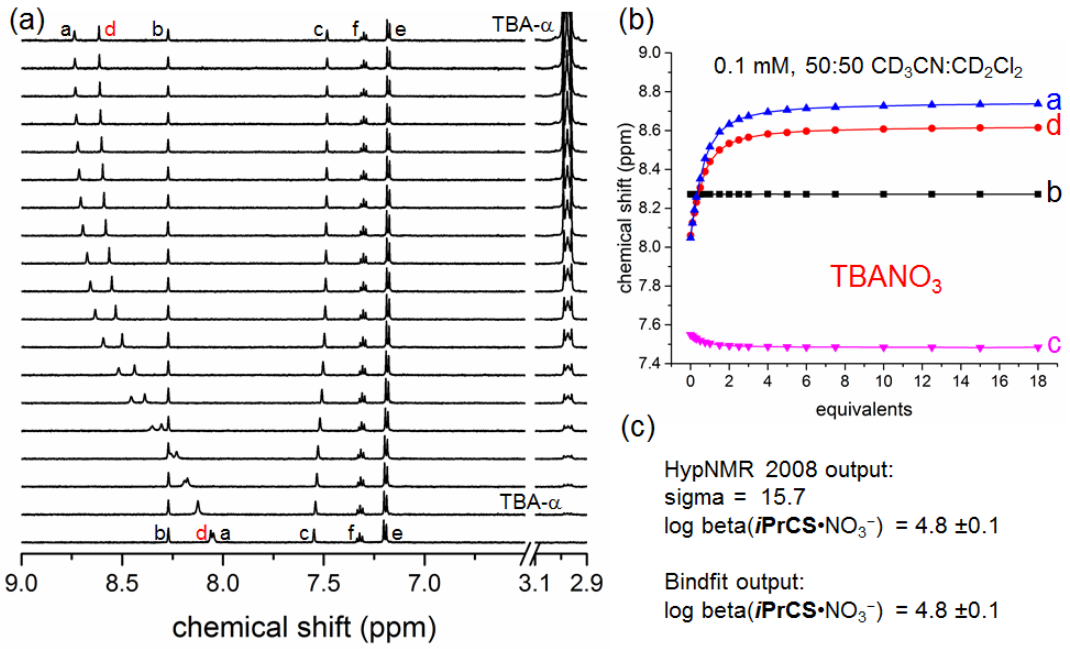

Figure S20. (a) Stacked ^{1}H NMR spectra and (b) cyanostar core protons' chemical shift positions connected by trend lines with increasing amount of $TBANO_3$ (1 mM ***i*PrCS**, 50:50 CD_3CN:CD_2Cl_2, 298 K, 600 MHz). (c) Fitting output from HypNMR 2008 and Bindfit.

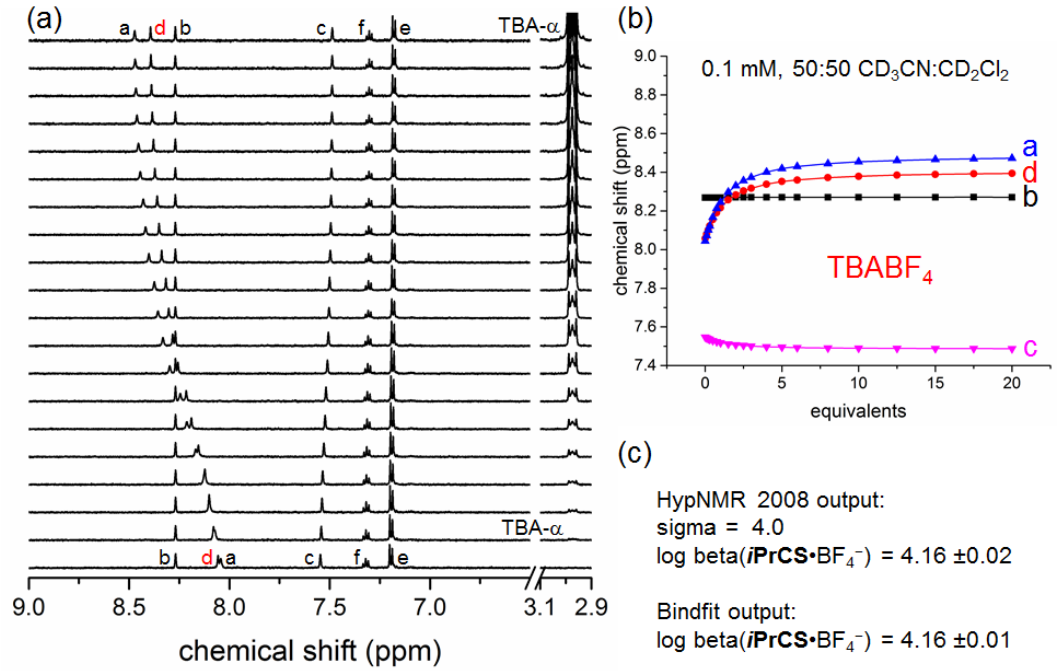

Figure S21. (a) Stacked ^{1}H NMR spectra and (b) cyanostar core protons' chemical shift positions connected by trend lines with increasing amount of $TBABF_4$ (1 mM ***i*PrCS**, 50:50 CD_3CN:CD_2Cl_2, 298 K, 600 MHz). (c) Fitting output from HypNMR 2008 and Bindfit.

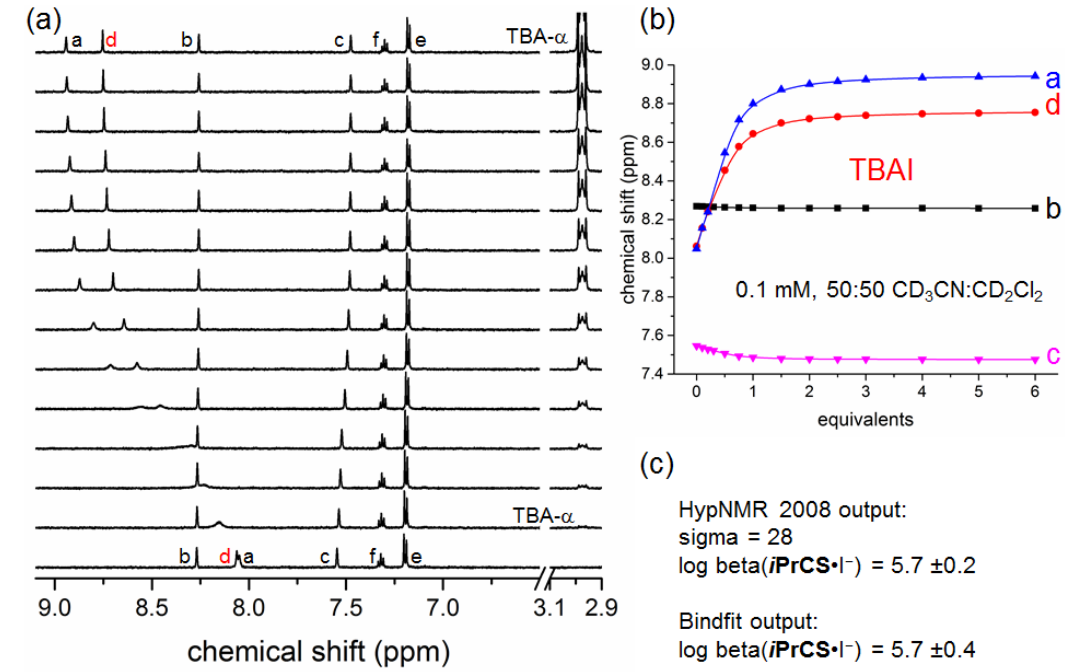

Figure S22. (a) Stacked ^{1}H NMR spectra and (b) cyanostar core protons' chemical shift positions connected by trend lines with increasing amount of TBAI (1 mM ***i*PrCS**, 50:50 CD_3CN:CD_2Cl_2, 298 K, 600 MHz). (c) Fitting output from HypNMR 2008 and Bindfit.

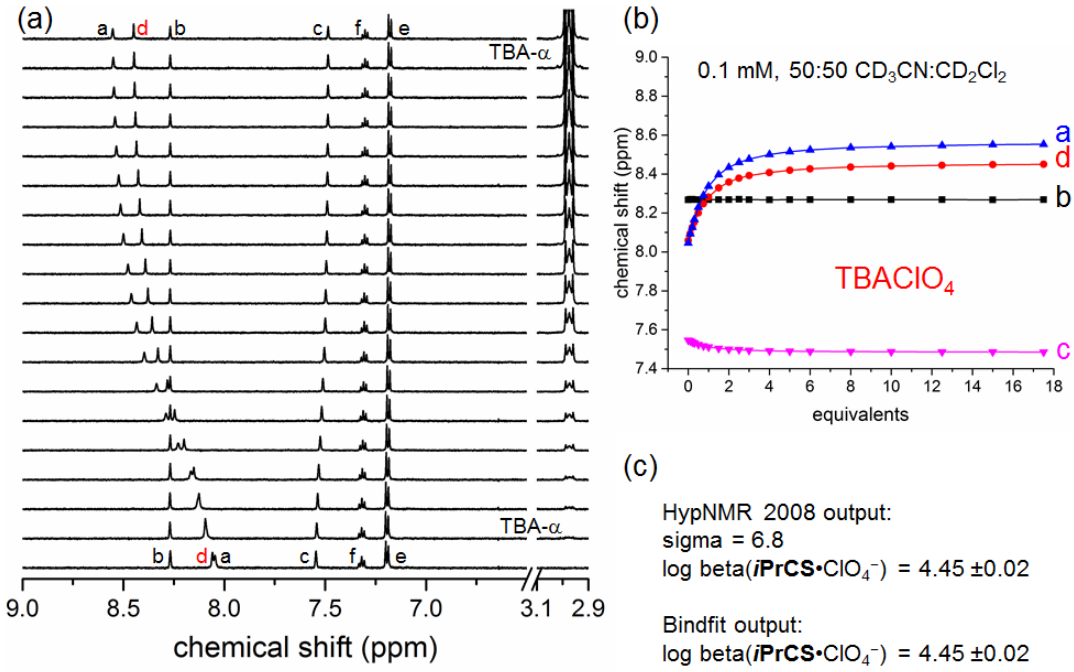

Figure S23. (a) Stacked ^{1}H NMR spectra and (b) cyanostar core protons' chemical shift positions connected by trend lines with increasing amount of $TBAClO_4$ (1 mM ***i*PrCS**, 50:50 CD_3CN:CD_2Cl_2, 298 K, 600 MHz). (c) Fitting output from HypNMR 2008 and Bindfit.

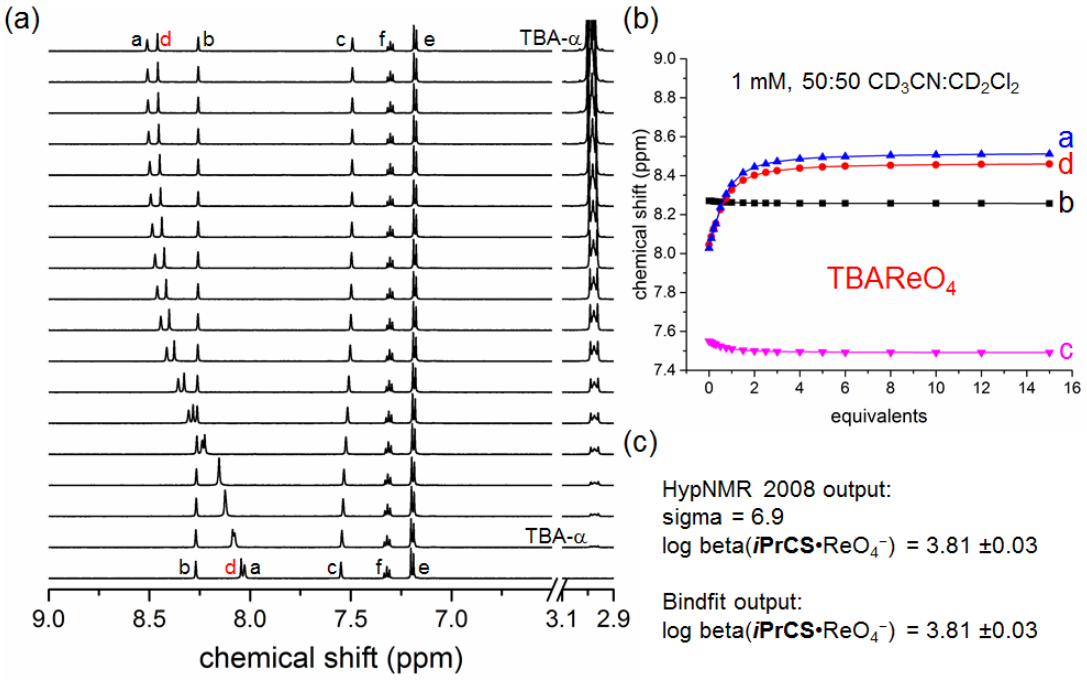

Figure S24. (a) Stacked ^{1}H NMR spectra and (b) cyanostar core protons' chemical shift positions connected by trend lines with increasing amount of $TBAReO_4$ (1 mM ***i*PrCS**, 50:50 CD_3CN:CD_2Cl_2, 298 K, 600 MHz). (c) Fitting output from HypNMR 2008 and Bindfit.

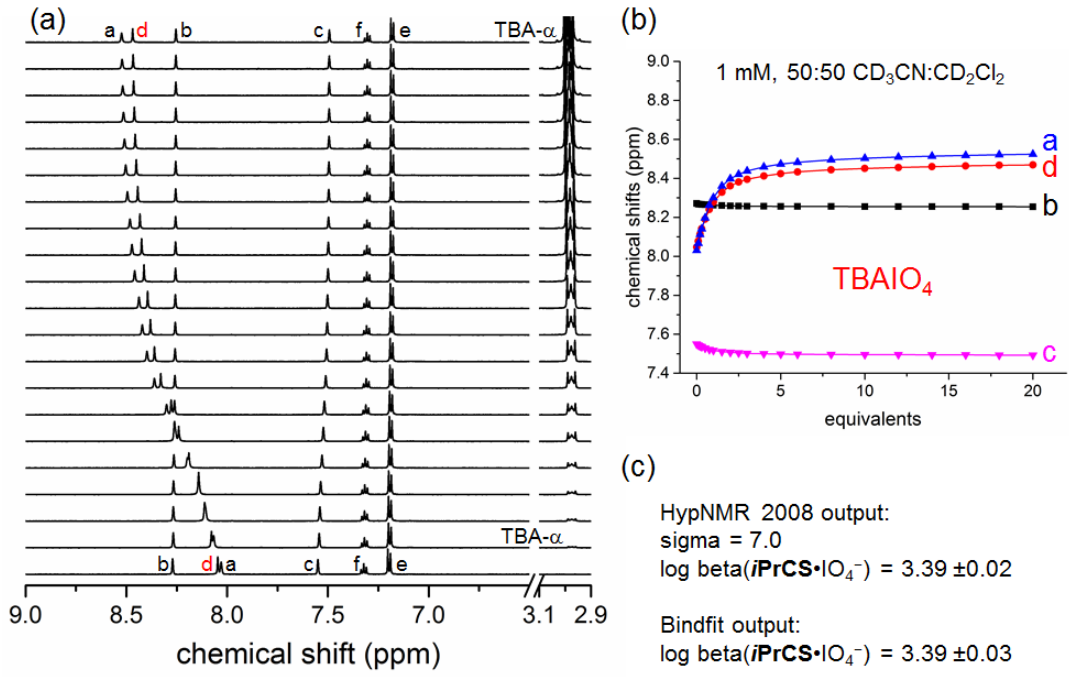

Figure S25. (a) Stacked ^{1}H NMR spectra and (b) cyanostar core protons' chemical shift positions connected by trend lines with increasing amount of $TBAIO_4$ (1 mM ***i*PrCS**, 50:50 CD_3CN:CD_2Cl_2, 298 K, 600 MHz). (c) Fitting output from HypNMR 2008 and Bindfit.

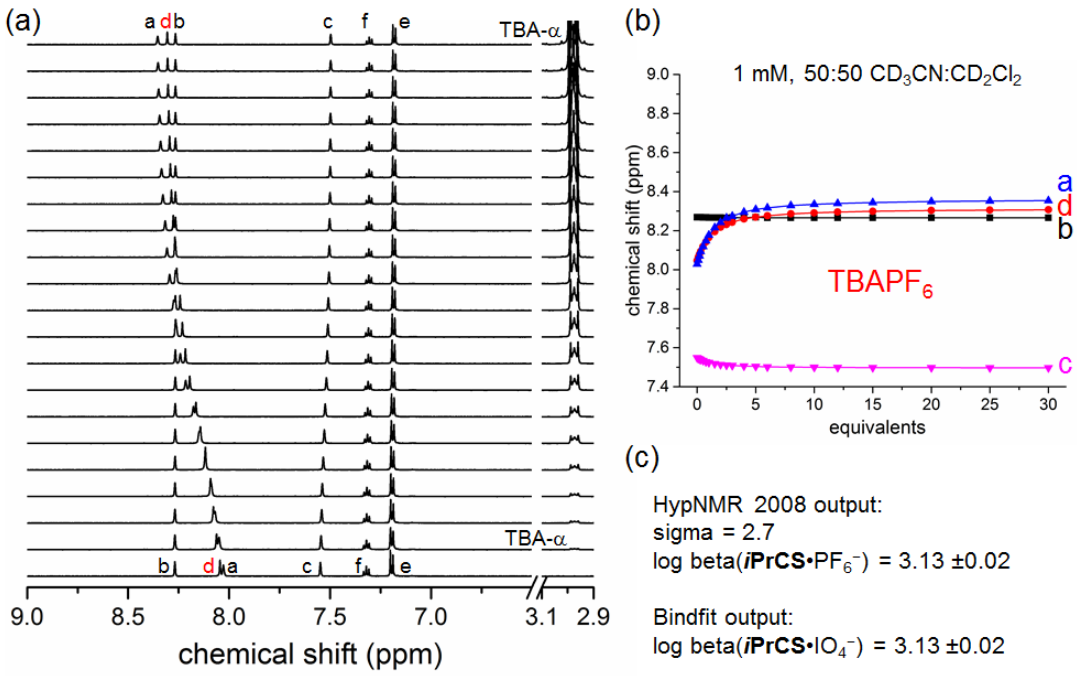

Figure S26. (a) Stacked ^{1}H NMR spectra and (b) cyanostar core protons' chemical shift positions connected by trend lines with increasing amount of $TBAPF_6$ (1 mM ***i*PrCS**, 50:50 CD_3CN:CD_2Cl_2, 298 K, 600 MHz). (c) Fitting output from HypNMR 2008 and Bindfit.

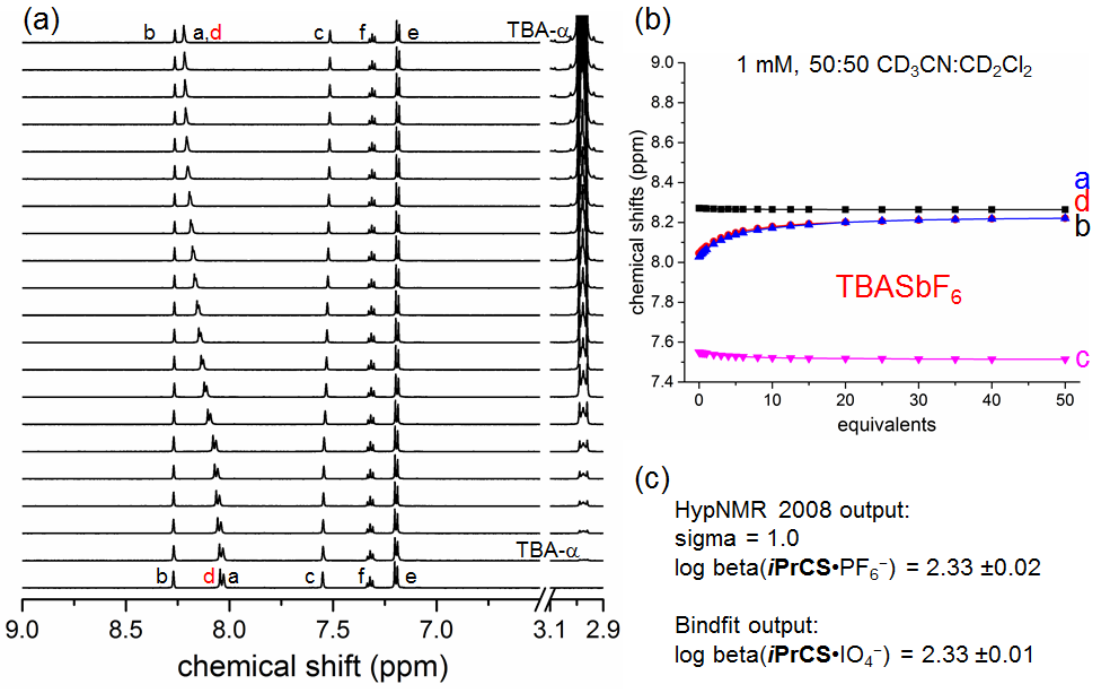

Figure S27. (a) Stacked ^{1}H NMR spectra and (b) cyanostar core protons' chemical shift positions connected by trend lines with increasing amount of $TBASbF_6$ (1 mM ***i*PrCS**, 50:50 CD_3CN:CD_2Cl_2, 298 K, 600 MHz). (c) Fitting output from HypNMR 2008 and Bindfit.

Table S3. Summary of the fitting results of ^{1}H NMR titrations.

solvent	anion	*c* (mM)	log *K* (Bindfit)	log *K* (HypNMR)	δH_a in ***i*PrCS**•X^- (HypNMR)	δH_d in ***i*PrCS**•X^- (HypNMR)	sigma (HypNMR)
	Cl^-	1	2.09 ±0.01	2.09 ±0.02	8.63	8.57	0.98
	Br^-	1	2.81 ±0.01	2.80 ±0.02	8.66	8.58	3.1
	NO_3^-	1	3.20 ±0.01	3.20 ±0.02	8.62	8.55	4.1
	BF_4^-	1	4.4 ±0.1	4.4 ±0.1	8.53	8.46	9.8
	I^-	1	4.6 ±0.2	4.6 ±0.1	8.92	8.75	16
40:60	I^-	0.1	4.41 ±0.02	4.38 ±0.01	8.92	8.76	6.3
$CD_3OD:CD_2Cl_2$	ClO_4^-	1	4.8 ±0.3	4.8 ±0.2	8.61	8.52	14
	$ClO4^-$	0.1	4.54 ±0.01	4.54 ±0.02	8.61	8.52	4.6
	ReO_4^-	1	3.48 ±0.02	3.48 ±0.02	8.52	8.49	5.2
	IO_4^-	1	3.12 ±0.01	3.12 ±0.02	8.52	8.49	2.2
	PF_6^-	1	3.92 ±0.03	3.92 ±0.02	8.42	8.38	3.5
	SbF_6^-	1	3.27 ±0.02	3.27 ±0.02	8.31	8.33	3.2
	Cl^-	1	2.89 ±0.02	2.89 ±0.02	8.75	8.63	4.2
	Br−	1	3.86 ±0.01	3.86 ±0.02	8.72	8.60	2.9
	NO_3^-	1	-	5.0 ±0.3	8.74	8.62	24
	NO_3^-	0.1	4.8 ±0.1	4.8 ±0.1	8.74	8.62	15.7
	BF_4^-	0.1	4.16 ±0.02	4.16 ±0.02	8.50	8.41	4.0
50:60	I^-	0.1	5.7 ±0.4	5.7 ±0.2	8.94	8.75	28
$CD_3CN:CD_2Cl_2$	ClO_4^-	1	-	5.0 ±0.3	8.57	8.46	20
	$ClO4^-$	0.1	4.45 ±0.01	4.45 ±0.02	8.57	8.46	6.8
	ReO_4^-	1	3.81 ±0.03	3.81 ±0.03	8.52	8.46	6.9
	IO_4^-	1	3.39 ±0.03	3.39 ±0.02	8.53	8.48	7.0
	PF_6^-	1	3.92 ±0.02	3.13 ±0.02	8.37	8.32	2.7
	SbF_6^-	1	2.33 ±0.01	2.33 ±0.02	8.27	8.27	1.0

Complexation Induced Shifts (CIS)

The chemical shift values for the cavity hydrogens of ***i*PrCS** (Figure S28) all move downfield upon complexation. This behavior is as expected: The proximity of hydrogens to negatively charged ions and their involvement in hydrogen bonding reduces the electron density around the proton, inducing greater deshielding effects. The CIS values for the two hydrogen-bonded protons (H_a and H_d) in the two solvent mixtures range from 0.2 to 0.9 ppm with H_a showing a CIS value that is 5-10% greater than H_d in both solvents. As noted by Hay[13] unpolarized phenylene CH donors can engage in hydrogen bonding but are weaker than polarized ones. Thus, this observation is consistent with H_a being closer to the center of the cavity; an effect of proximity and not hydrogen bonding strength. This observation, therefore, is the first observation that is against the simpler idea that CIS correlates with hydrogen bond strengths.

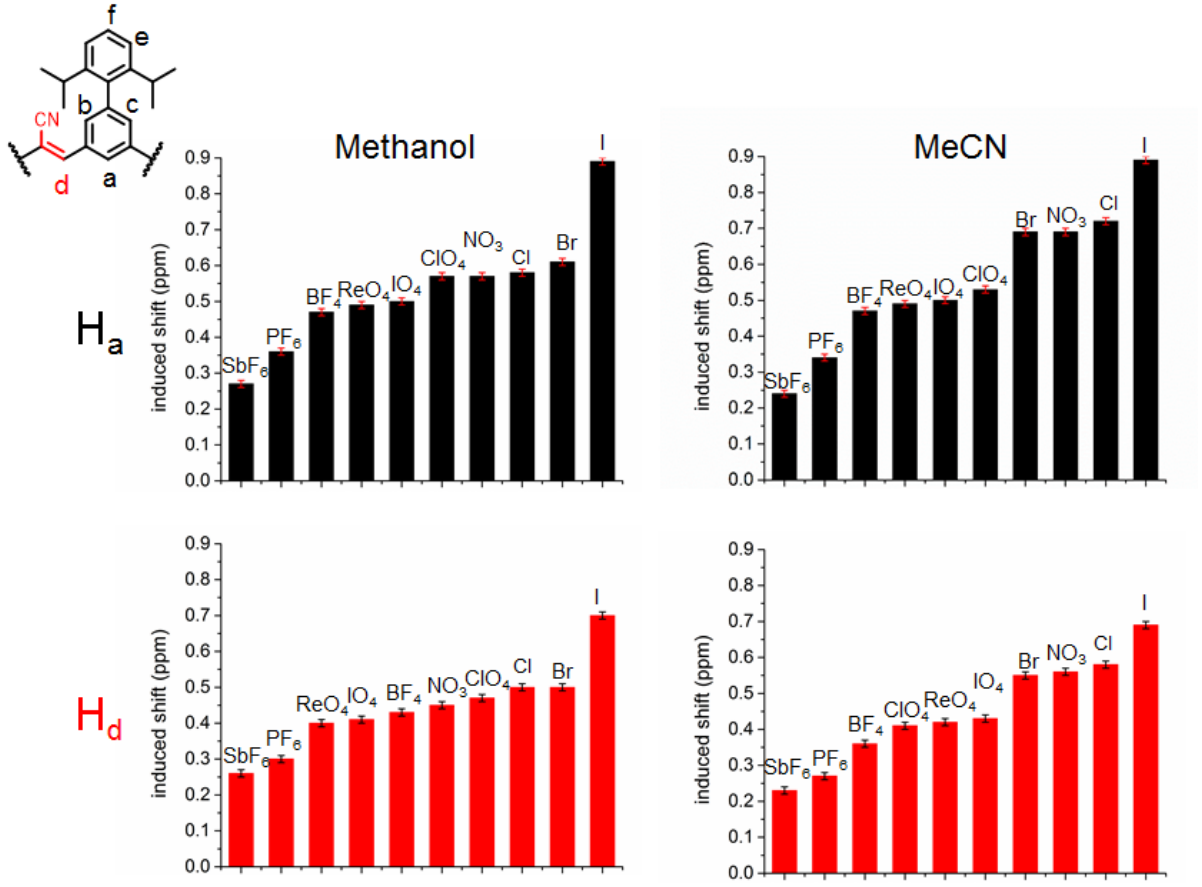

Figure S28. Anion complexation induced chemical shifts (CIS) on H_a and H_d. Values were calculated using equation: CIS = δ[H_x in ***i*PrCS**•anion] – δ[H_x in ***i*PrCS**], where δ[H_x in ***i*PrCS**] are experimental values and δ[H_x in ***i*PrCS**•anion] were obtained from the fittings by HypNMR.

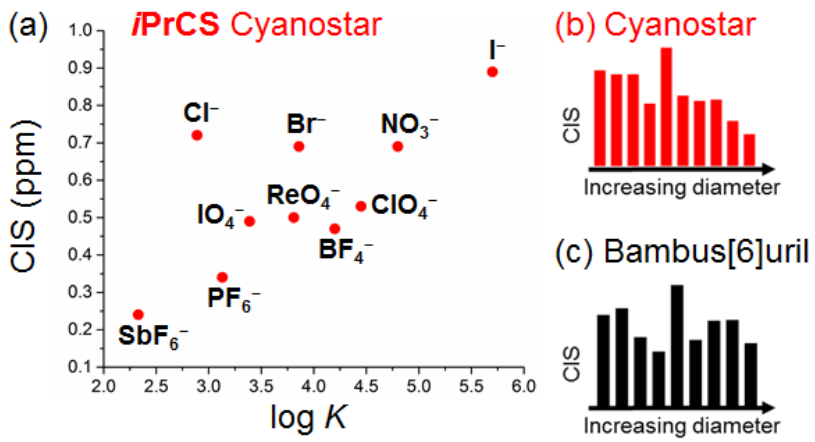

Figure S29. Complexation induced shifts (CIS) of H_a in 50:50 CD_3CN:CD_2Cl_2 plotted as a function of (a) log value of 1:1 affinity (*K*) and (b) anion diameter. (c) CIS-diameter plot of bambus[6]uril NH proton in $CHCl_3$.

Contrary to common wisdom, the data (Figure S29a) show that anion binding strength is not correlated with CIS values. When the CIS values are listed in order of increasing anion diameter for ***i*PrCS** and bambus[6]uril (Fig. S29b and S29c), there is still no correlation. For cyanostar, it is noticed that the small and hard anions (Cl^-, Br^-, and NO_3^-) all induce high shifts, presumably because of the strong electrostatic field around them. Iodide has the highest CIS most likely resulting from the best size matching with the macrocycle. The tetrahedral anions induce lower shifts and the larger and octahedral anions show CIS values that are smaller again. However, when CIS values are plotted as a function of binding affinities, there is no obvious trend. All the observations indicate that CIS does not genuinely reflect binding strength and behoove us to postulate more sophisticated explanations for the observed CIS values. We are currently studying the geometry of the macrocycle-anions complexes using crystallography and density function theory to test the hypothesized explanations for CIS.

Additional Binding Data and Fitting Results

To further verify the biased solvation effect, we preformed several extra titrations in two other solvent systems: 50:50 *v*/*v* dichloromethane:acetone (aprotic, ε_{eff} = 15) and 50:50 *v*/*v* chloroform:ethanol (protic, ε_{eff} = 15). The anions tested in these two solvent systems are I^-, ClO_4^-, IO_4^-, and PF_6^- with increasing diameter. The results (Figure S30-S38) match with those observed for the initial aprotic and protic solvent systems (Figure 30c and d). Thus, our results are consistent with the hypothesis that size-selectivity is distorted in protic and retained in aprotic solvent mixtures. For example, in the protic chloroform:ethanol solvent mixture the affinity for PF_6^- exceeds the smaller IO_4^-, while in the aprotic dichloromethane:acetone solvent mixture IO_4^- binds stronger than PF_6^-.

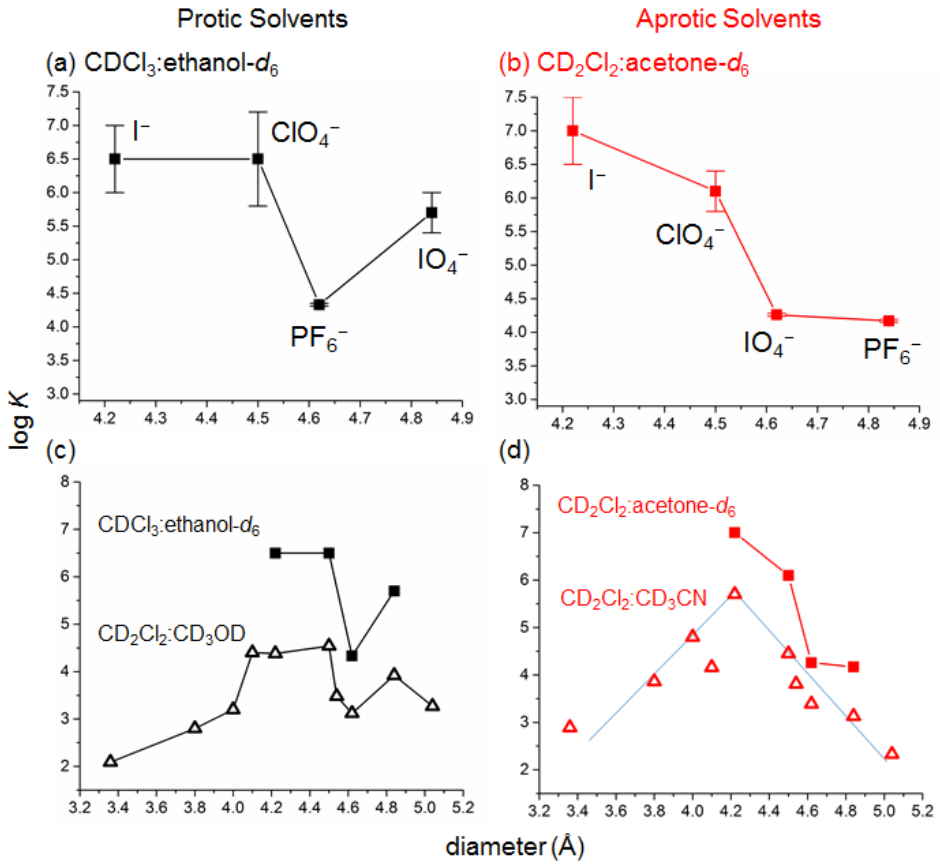

Figure S30. Association constants (log *K*) of ***i*PrCS** in (a) 50:50 $CDCl_3$:ethanol-d_6 and (b) 50:50 CD_2Cl_2:acetone-d_6. (c) Comparison of the anion-binding log *K* values of ***i*PrCS** in 50:50 $CDCl_3$:ethanol-d_6 (black squares) and in 60:40 CD_2Cl_2:CD_3OD (black triangles). (d) Comparison of the anion-binding log *K* values of ***i*PrCS** in 50:50 CD_2Cl_2:acetone-d_6 (red squares) and in 50:50 CD_2Cl_2:CD_3CN (red triangles).

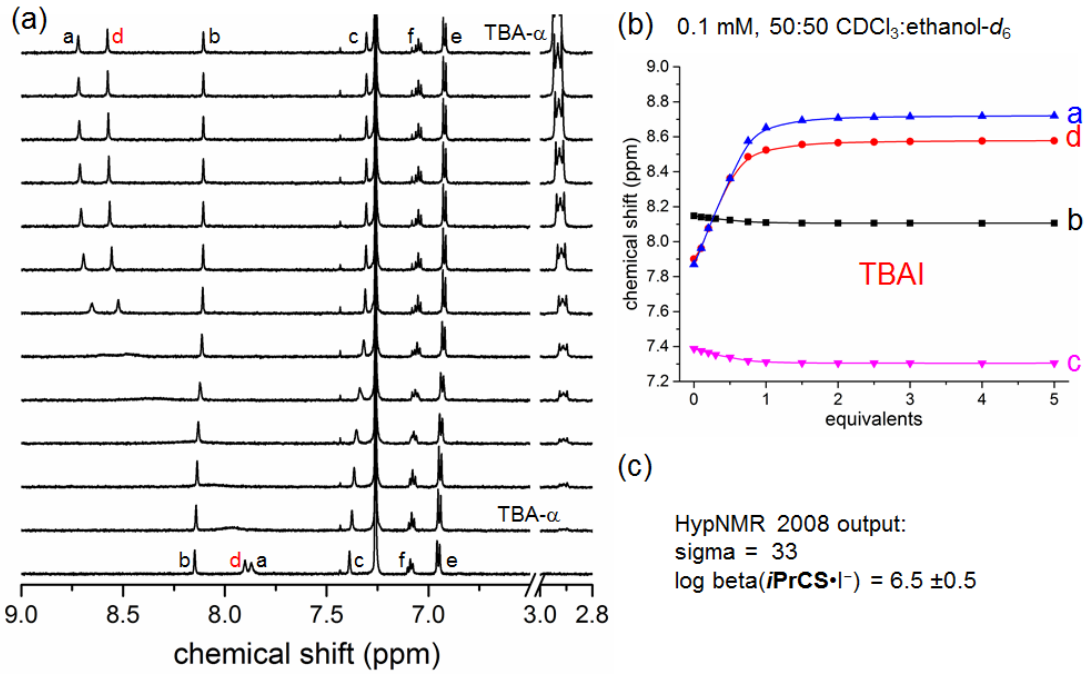

Figure S31. (a) Stacked ^{1}H NMR spectra and (b) cyanostar core protons' chemical shift positions connected by trend lines with increasing amount of TBAI (0.1 mM ***i*PrCS**, 50:50 $CDCl_3$:ethanol-d_6, 298 K, 600 MHz). (c) Fitting output from HypNMR 2008.

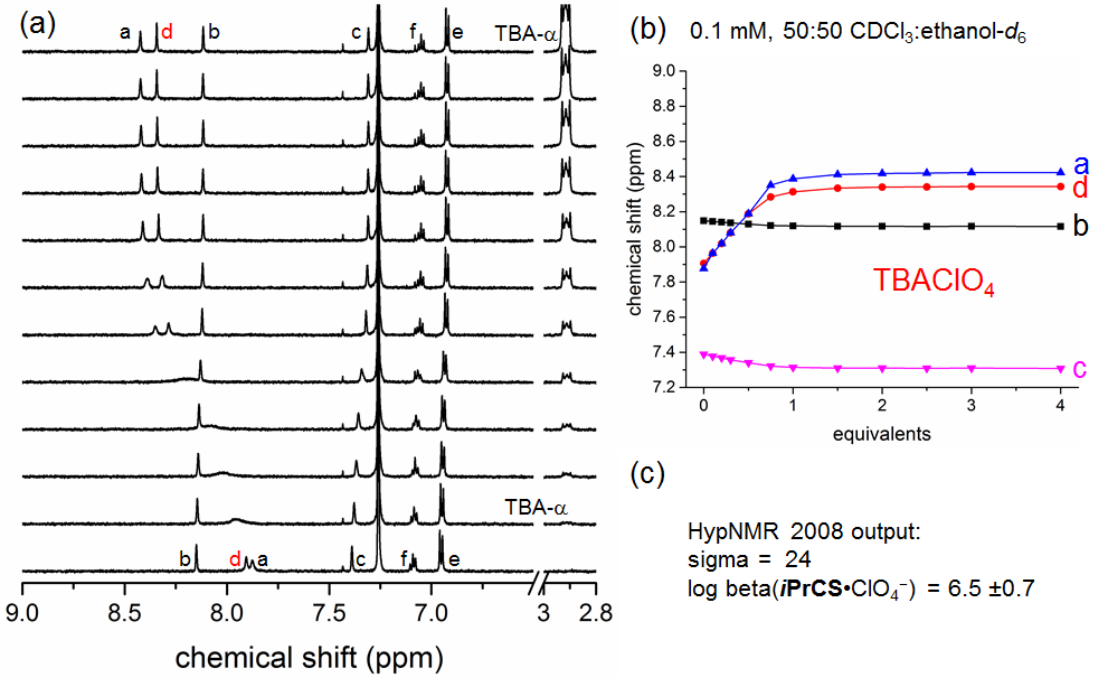

Figure S32. (a) Stacked ^{1}H NMR spectra and (b) cyanostar core protons' chemical shift positions connected by trend lines with increasing amount of $TBAClO_4$ (0.1 mM ***i*PrCS**, 50:50 $CDCl_3$:ethanol-d_6, 298 K, 600 MHz). (c) Fitting output from HypNMR 2008.

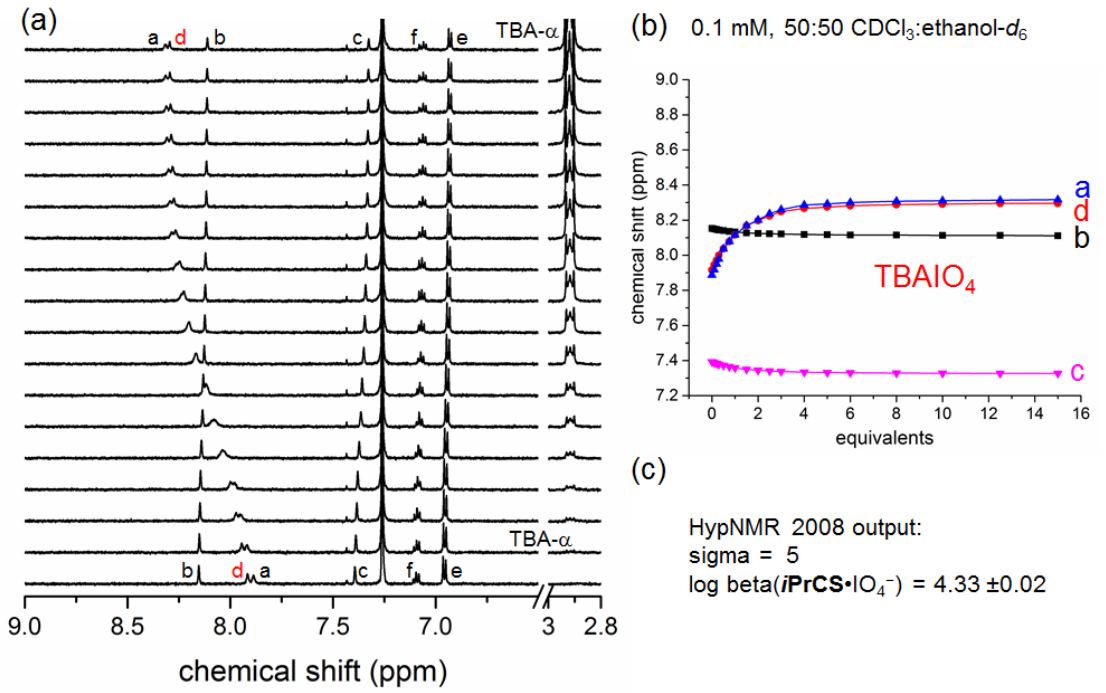

Figure S33. (a) Stacked ^{1}H NMR spectra and (b) cyanostar core protons' chemical shift positions connected by trend lines with increasing amount of $TBAIO_4$ (0.1 mM ***i*PrCS**, 50:50 $CDCl_3$:ethanol-d_6, 298 K, 600 MHz). (c) Fitting output from HypNMR 2008.

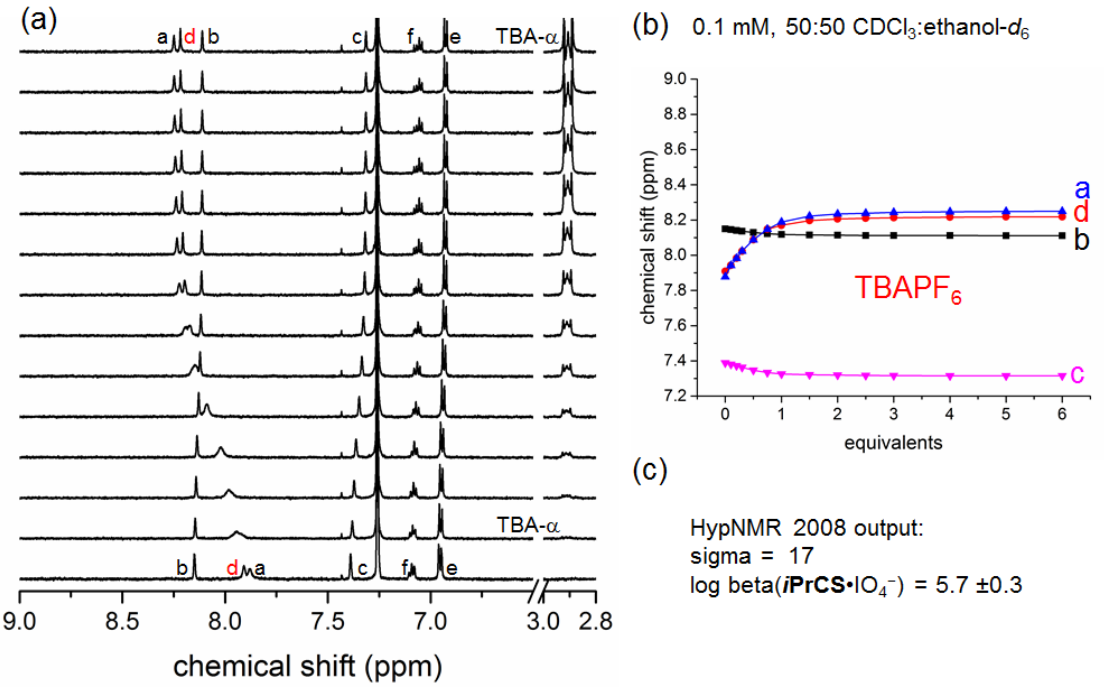

Figure S34. (a) Stacked ^{1}H NMR spectra and (b) cyanostar core protons' chemical shift positions connected by trend lines with increasing amount of $TBAPF_6$ (0.1 mM ***i*PrCS**, 50:50 $CDCl_3$:ethanol-d_6, 298 K, 600 MHz). (c) Fitting output from HypNMR 2008.

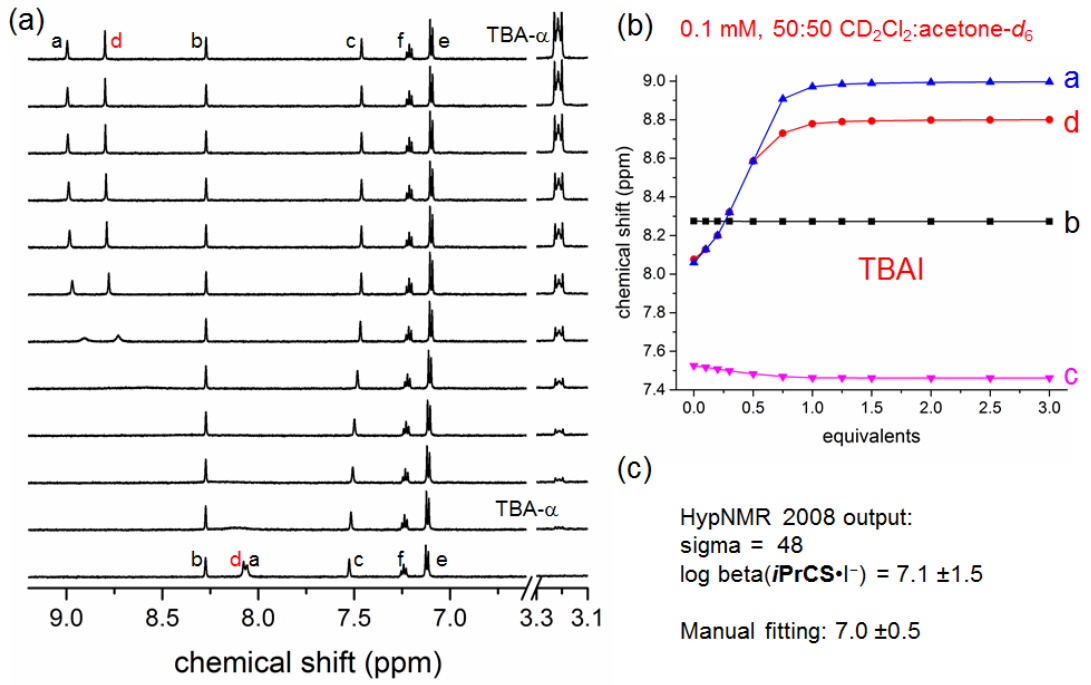

Figure S35. (a) Stacked ^{1}H NMR spectra and (b) cyanostar core protons' chemical shift positions connected by trend lines with increasing amount of TBAI (0.1 mM ***i*PrCS**, 50:50 CD_2Cl_2:acetone-d_6, 298 K, 600 MHz). (c) Fitting output from HypNMR 2008.

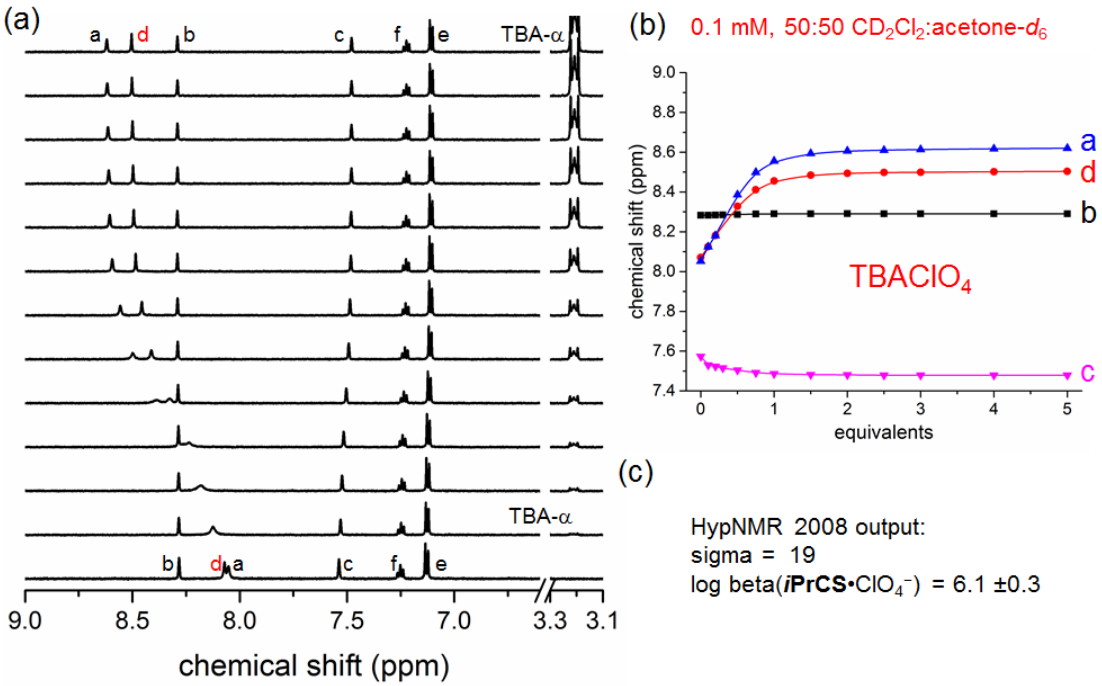

Figure S36. (a) Stacked ^{1}H NMR spectra and (b) cyanostar core protons' chemical shift positions connected by trend lines with increasing amount of $TBAClO_4$ (0.1 mM ***i*PrCS**, 50:50 CD_2Cl_2:acetone-d_6, 298 K, 600 MHz). (c) Fitting output from HypNMR 2008.

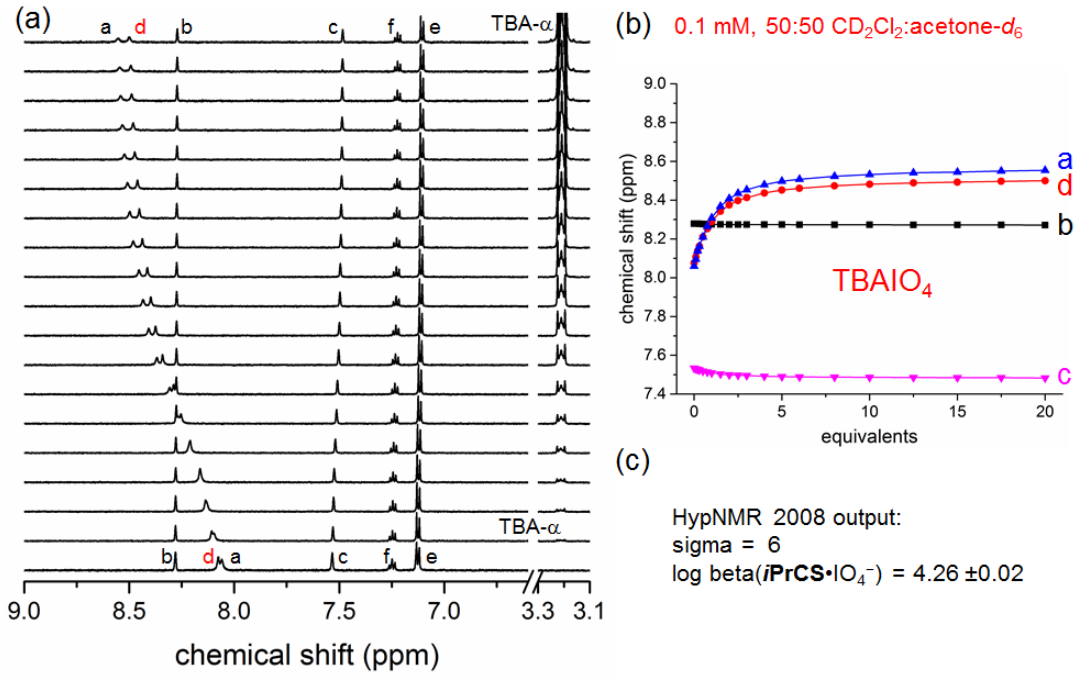

Figure S37. (a) Stacked ^{1}H NMR spectra and (b) cyanostar core protons' chemical shift positions connected by trend lines with increasing amount of $TBAIO_4$ (0.1 mM ***i*PrCS**, 50:50 CD_2Cl_2:acetone-d_6, 298 K, 600 MHz). (c) Fitting output from HypNMR 2008.

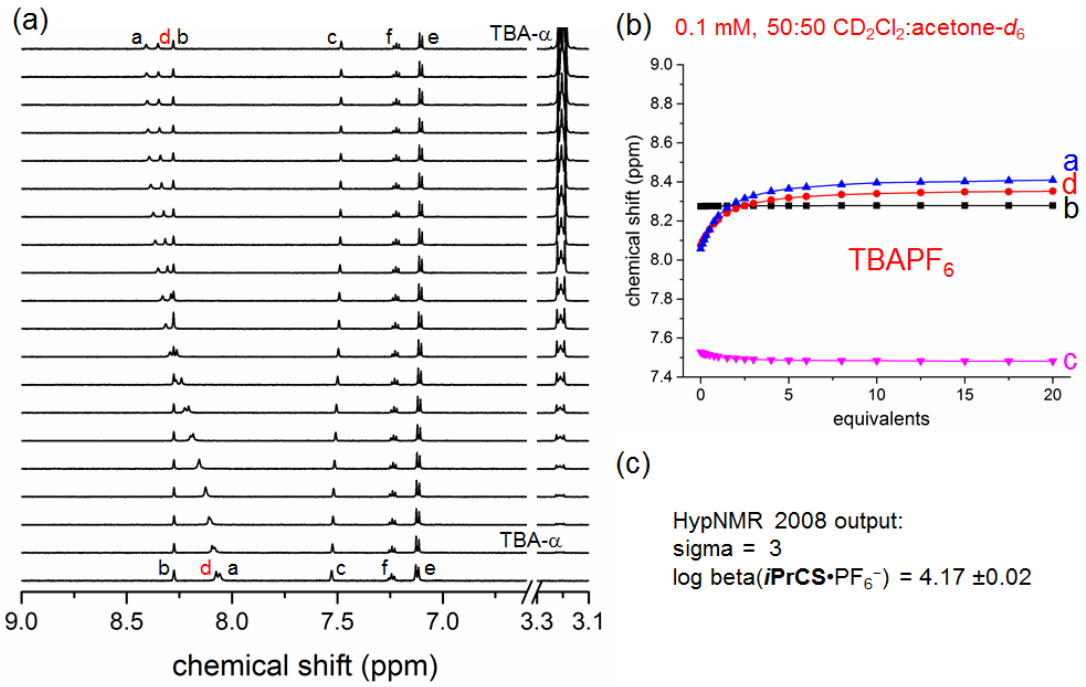

Figure S38. (a) Stacked ^{1}H NMR spectra and (b) cyanostar core protons' chemical shift positions connected by trend lines with increasing amount of $TBAPF_6$ (0.1 mM ***i*PrCS**, 50:50 CD_2Cl_2:acetone-d_6, 298 K, 600 MHz). (c) Fitting output from HypNMR 2008.

S9. Analysis of Solvent Quality and Solvation of Anions

Hydrogen-Bond Donor Character of Solvents

Table S4. Acceptor number (AN) of related solvents

solvent	AN
water	55
methanol	42
chloroform	23
dichloromethane	20
acetonitrile	19
1,2-dichloroethane	17

The acceptor number (AN) of various solvents (Table S4) helps consider differences and similarities between methanol and acetonitrile. The AN value is measured by the Gutmann-Beckett method[14,15] to assess a molecule's ability of accepting electrons from triethylphosphine oxide. The AN value of water, methanol and chloroform are greater than dichloromethane, and acetonitrile. Chloroform has a weaker AN than water and methanol, but is still stronger than dichloromethane and acetonitrile.

Solvation of Anions in Different Solvents

Table S5. Solvation energy (kJ mol^{-1}) of anions in methanol and acetonitrile[16,17]

	$\Delta G_{sol}[CH_3OH]$	$\Delta G_{sol}[CH_3CN]$
Cl^-	−327	−298
Br^-	−284	−264
NO_3^-	−288	−279
I^-	−268	−258
ClO_4^-	−199	−203

S10. ^{1}H and ^{13}C NMR Spectra (* denotes impurities)

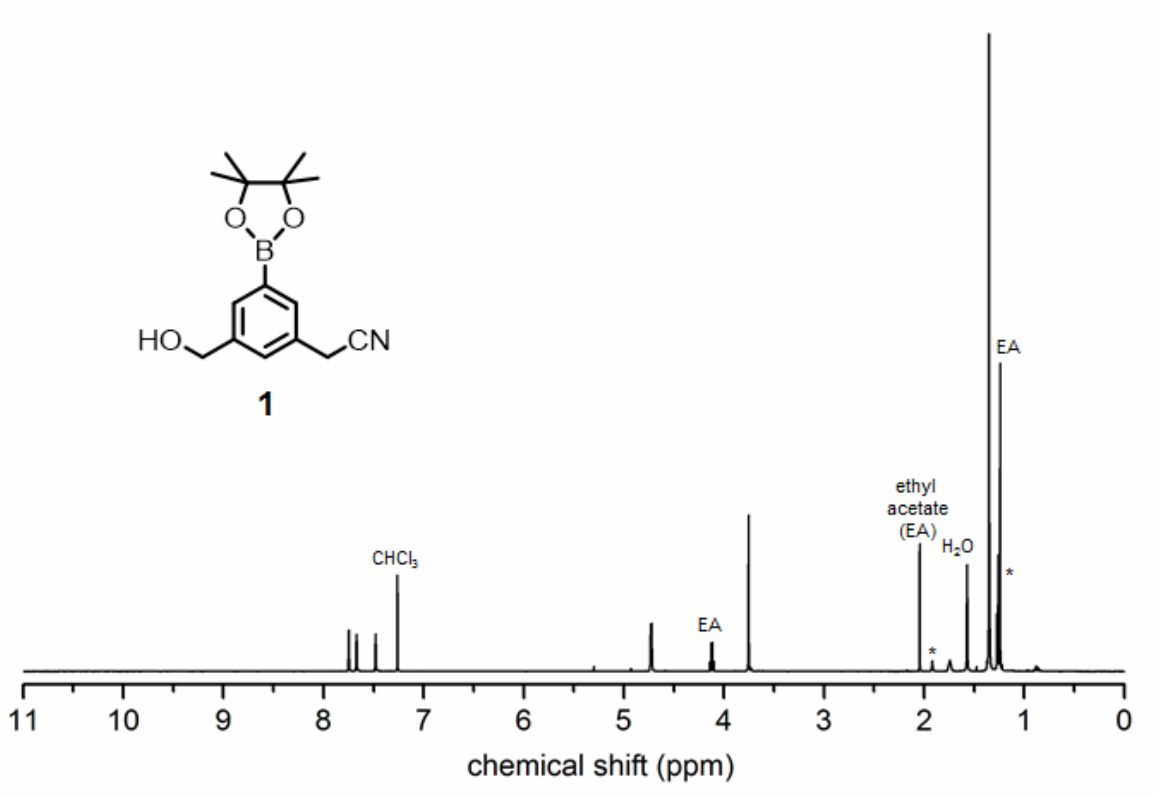

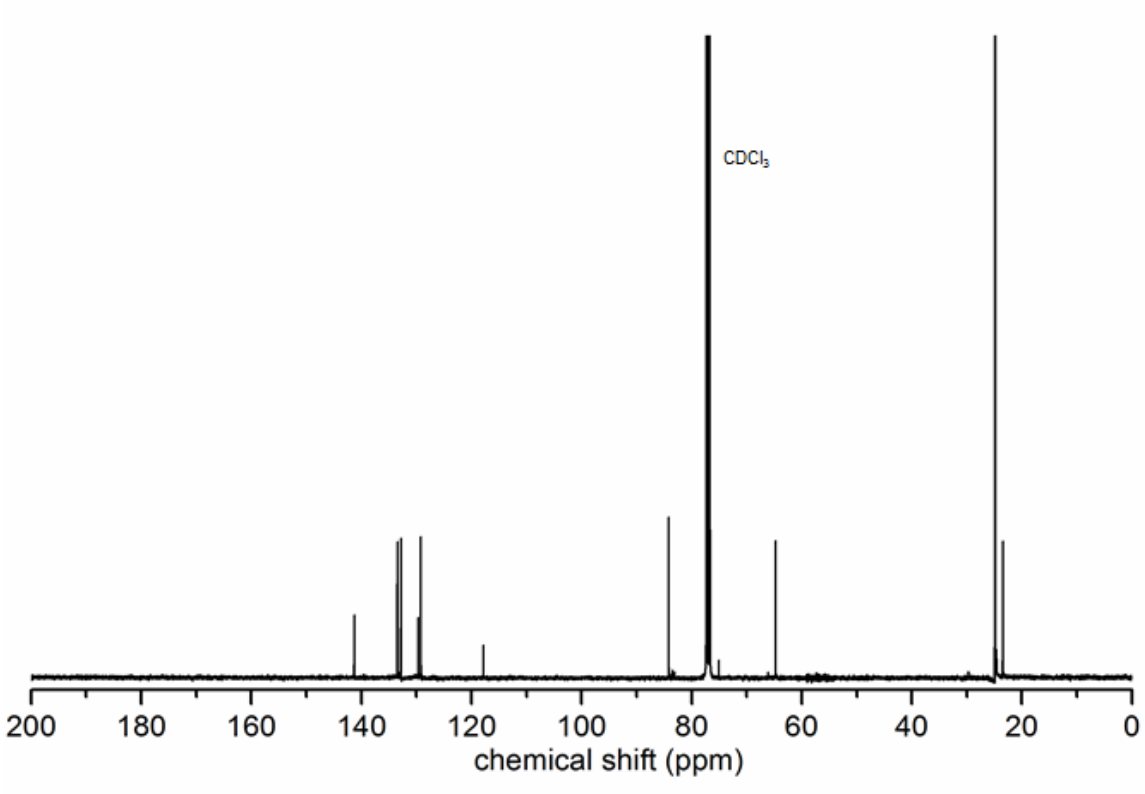

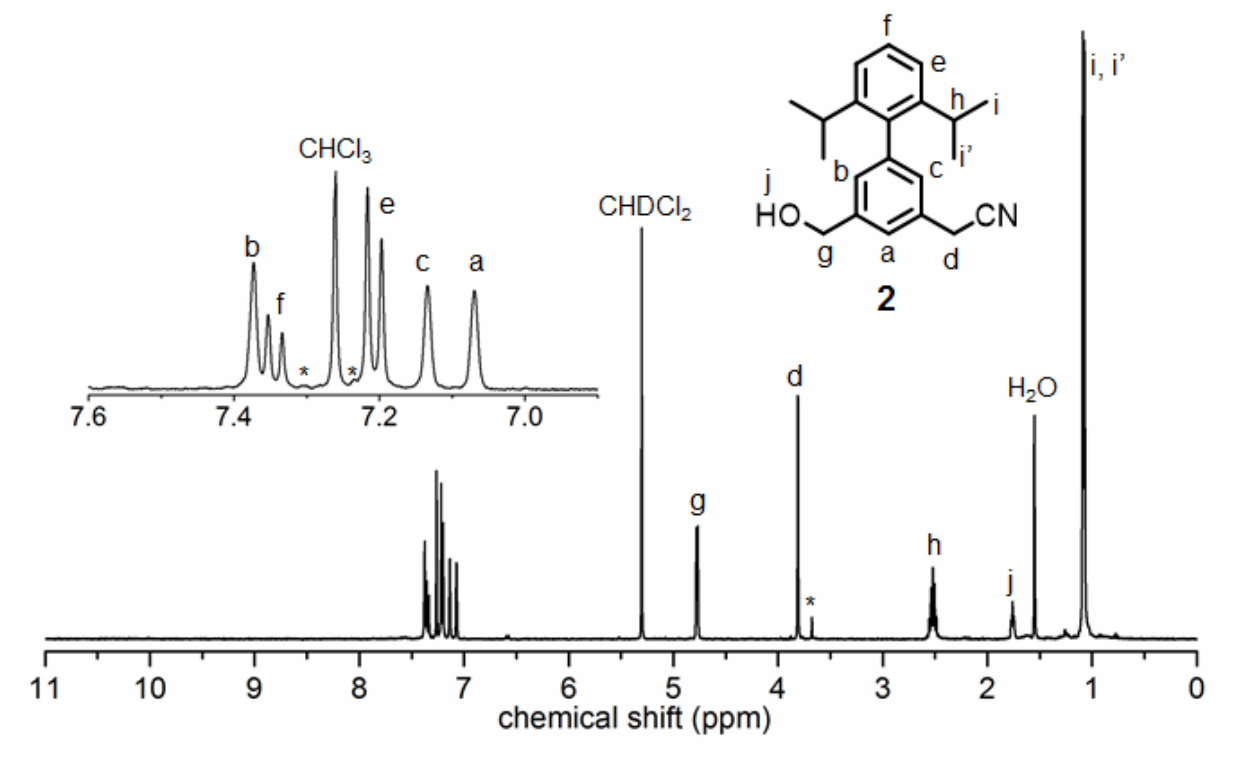
f
e
h
i
i'
b
c
j
HO
CN
g
a
d
2
i, i'
CHCl3
CHDCl2
H2O
b
f
e
c
a
d
g
h
j
*
7.6
7.4
7.2
7.0
11
10
9
8
7
6
5
4
3
2
1
0
chemical shift (ppm)

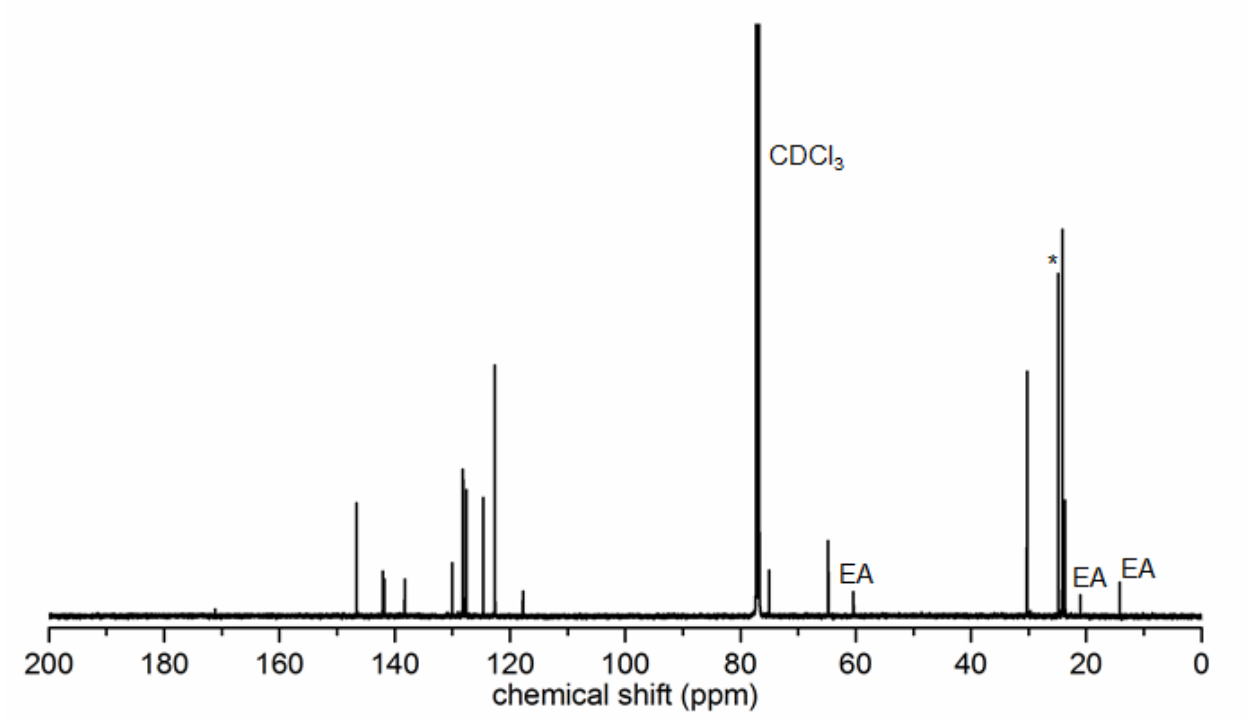
CDCl3
*
EA
EA
EA
200
180
160
140
120
100
80
60
40
20
0
chemical shift (ppm)

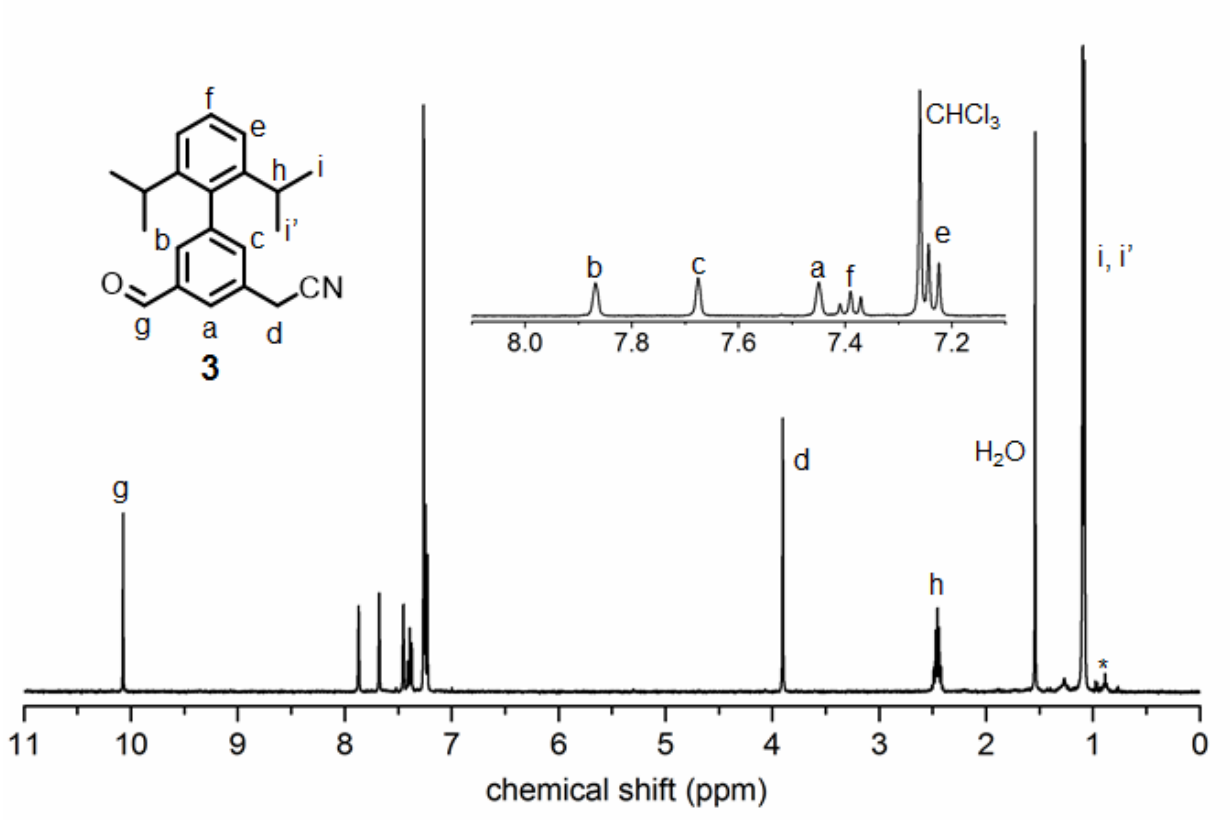
f
e
h
i
i'
b
c
O
CN
g
a
d
3
CHCl3
b
c
a
f
e
8.0
7.8
7.6
7.4
7.2
i, i'
H2O
d
g
h
*
11
10
9
8
7
6
5
4
3
2
1
0
chemical shift (ppm)

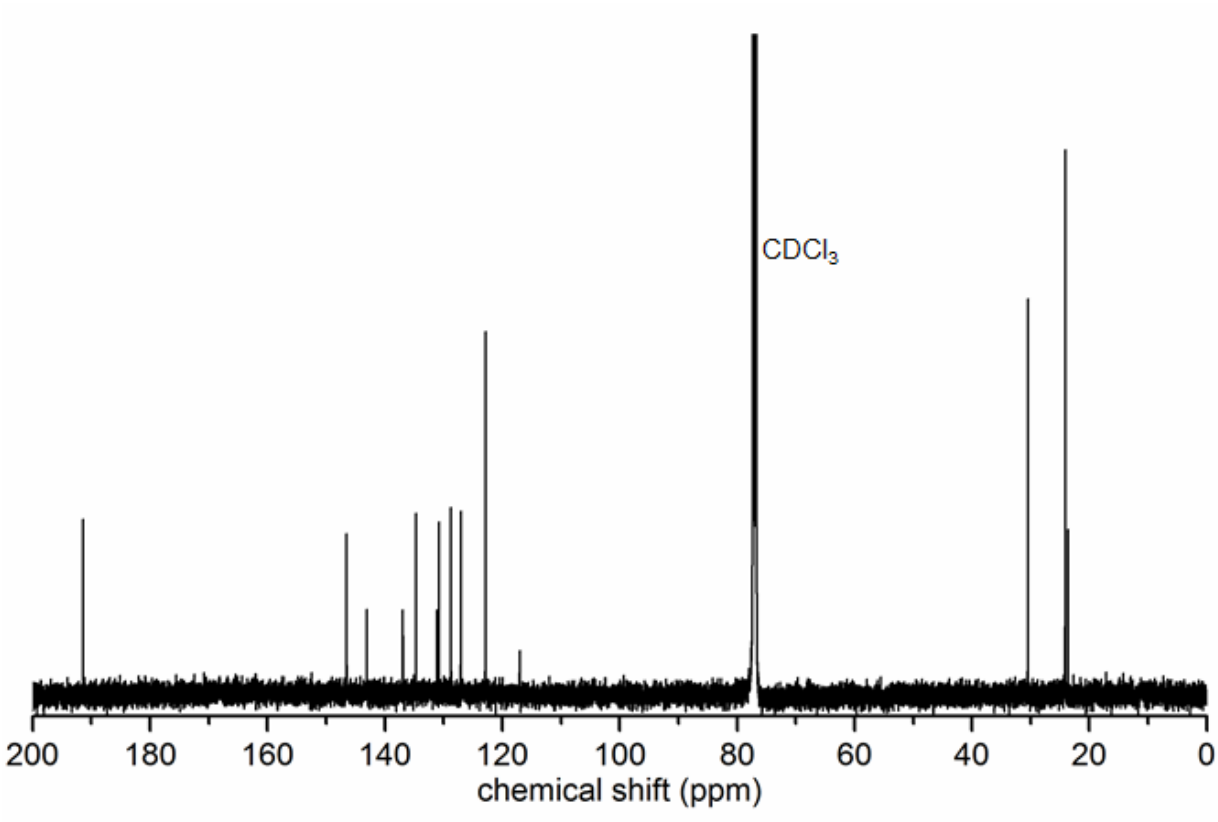
CDCl3
200
180
160
140
120
100
80
60
40
20
0
chemical shift (ppm)

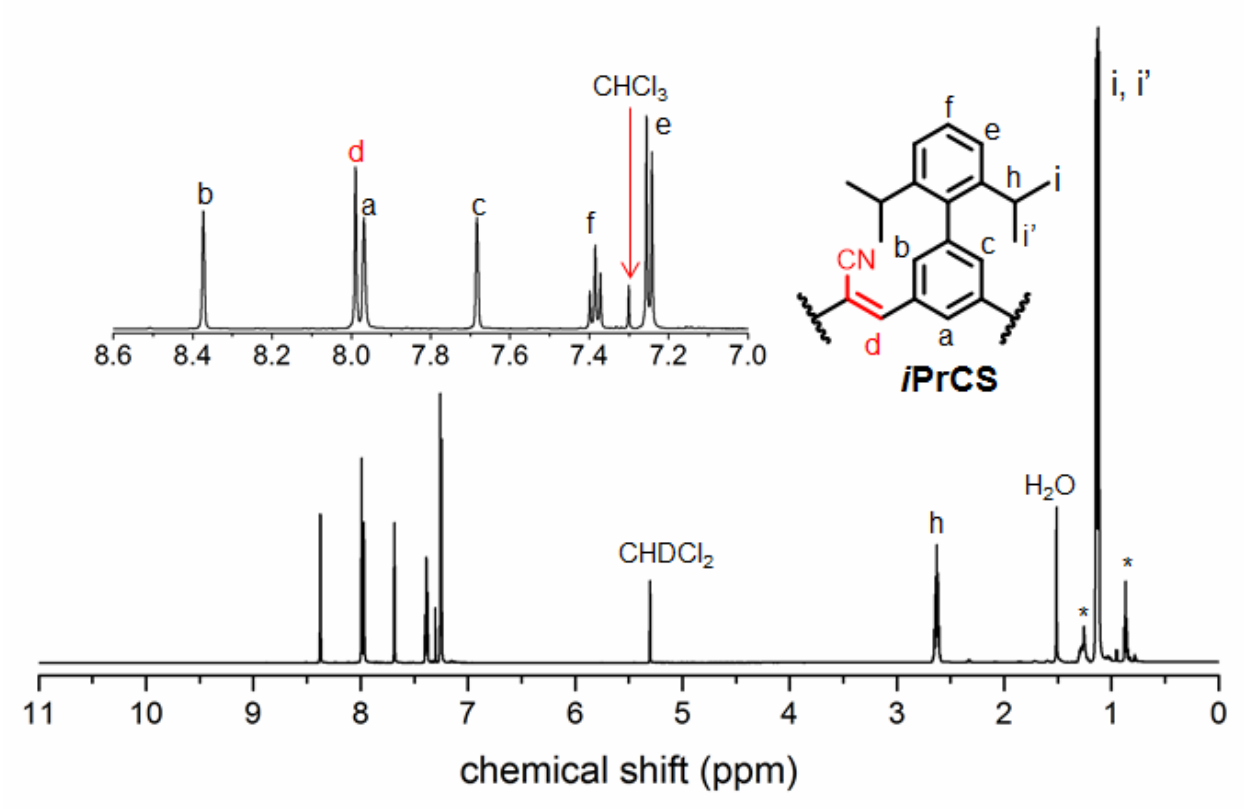
CHCl3
d
b
a
c
f
e
8.6
8.4
8.2
8.0
7.8
7.6
7.4
7.2
7.0
f
e
h
i
i'
b
c
CN
d
a
iPrCS
i, i'
H2O
h
CHDCl2
*
*
11
10
9
8
7
6
5
4
3
2
1
0
chemical shift (ppm)

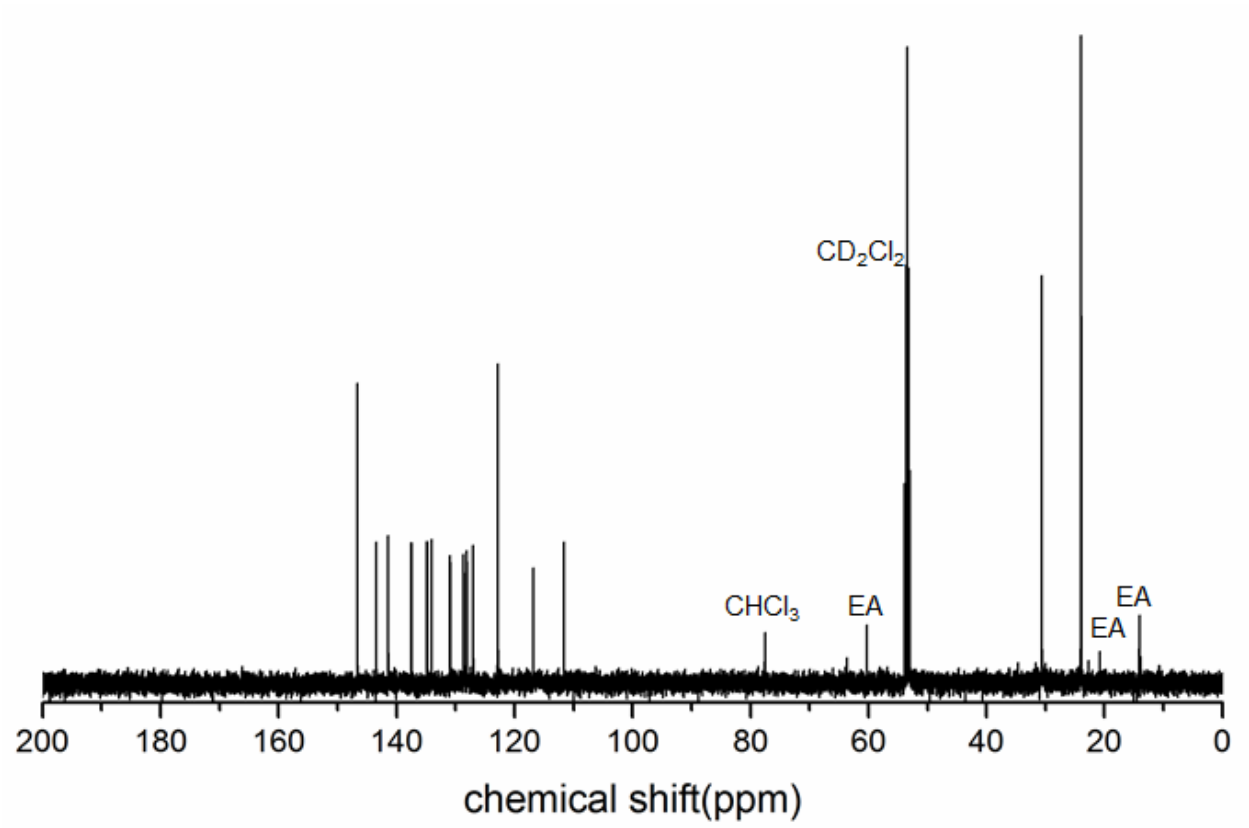
CD2Cl2
CHCl3
EA
EA
EA
200
180
160
140
120
100
80
60
40
20
0
chemical shift(ppm)

1. B. E. Hirsch, S. Lee, B. Qiao, C.-H. Chen, K. P. McDonald, S. L. Tait and A. H. Flood, *Chem. Commun.*, 2014, **50**, 9827-9830.
2. D. B. Bolstad, E. S. D. Bolstad, K. M. Frey, D. L. Wright and A. C. Anderson, *J. Med. Chem.*, 2008, **51**, 6839-6852.
3. S. E. Wheeler, *J. Am. Chem. Soc.*, 2011, **133**, 10262-10274.
4. SAINT, Bruker Analytical X-Ray Systems, Madison, WI, current version.
5. R. Blessing, *Acta. Cryst. A*, 1995, **51**, 33-38.
6. G. M. Sheldrick, *Acta Cryst. A*, 2008, **64**, 112-122.
7. *J. Mol. Biol.*, 1975, **91**, 201-225.
8. A. L. Spek, *Acta. Cryst.* D, 2009, **65**, 148-155.
9. R. S. Rowland and R. Taylor, *J. Phys. Chem.*, 1996, **100**, 7384-7391.
10. C. Frassineti, S. Ghelli, P. Gans, A. Sabatini, M.S. Moruzzi and A. Vacca, *Anal. Biochem.*, 1995, **231**, 374-382.
11. http://supramolecular.org
12. P. Thordarson, *Chem. Soc. Rev.*, 2011, **40**, 1305-1323.
13. V. S. Bryantsev and B. P. Hay, *J. Am. Chem. Soc.*, 2005, **127**, 8282-8283.
14. U. Mayer, V. Gutmann and W. Gerger, *Chemical Monthly*, 1975, **106**, 1235-1257.
15. M. A. Beckett, G. C. Strickland, J. R. Holland and K. Sukumar Varma, *Polymer*, 1996, **37**, 4629-4631.
16. (a) Y. Marcus, *J. Chem. Soc., Faraday Trans.*, 1991, **87**, 2995-2999. (b) Y. Marcus, M. J. Kamlet and R. W. Taft, *J. Phys. Chem.*, 1988, **92**, 3613-3622.
17. L. J. Sanchez Vallejo, J. M. Ovejero, R. A. Fernández and S. A. Dassie, *Int. J. Electrochemistry*, 2012, **2012**, 1-34.